



- Título artículo / Títol article: Toward Understanding the Photocatalytic Activity of PbMoO_4 Powders with Predominant (111), (100), (011), and (110) Facets. A Combined Experimental and Theoretical Study
- Autores / Autors Bomio, M. R. D. ; Tranquilin, R. L. ; Motta, F. V. ; Paskocimas, C. A. ; Nascimento, R. M. ; Gracia Edo, Lourdes ; Andrés Bort, Juan ; Longo, E.
- Revista: The Journal of Physical Chemistry C (2013) vol. 117, no 41
- Versión / Versió: Postprint
- Cita bibliográfica / Cita bibliogràfica (ISO 690): BOMIO, M. R. D., et al. Toward Understanding the Photocatalytic Activity of PbMoO_4 Powders with Predominant (111),(100),(011), and (110) Facets. A Combined Experimental and Theoretical Study. The Journal of Physical Chemistry C, 2013, vol. 117, no 41, p. 21382-21395.
- url Repositori UJI: <http://hdl.handle.net/10234/91090>

Towards Understanding the Photocatalytic Activity of PbMoO Powders with Predominant (111), (100), (011), and (110) facets. A Combined Experimental and Theoretical Study

Mauricio Bomio, Ricardo L Tranquilin, Fabiana Villela Motta, Carlos Alberto Paskocimas, Rubens Maribondo Nascimento, Lourdes Gracia, Juan Andrés, and Elson Longo

J. Phys. Chem. C, **Just Accepted Manuscript** • DOI: 10.1021/jp407416h • Publication Date (Web): 12 Sep 2013

Downloaded from <http://pubs.acs.org> on September 16, 2013

Just Accepted

“Just Accepted” manuscripts have been peer-reviewed and accepted for publication. They are posted online prior to technical editing, formatting for publication and author proofing. The American Chemical Society provides “Just Accepted” as a free service to the research community to expedite the dissemination of scientific material as soon as possible after acceptance. “Just Accepted” manuscripts appear in full in PDF format accompanied by an HTML abstract. “Just Accepted” manuscripts have been fully peer reviewed, but should not be considered the official version of record. They are accessible to all readers and citable by the Digital Object Identifier (DOI®). “Just Accepted” is an optional service offered to authors. Therefore, the “Just Accepted” Web site may not include all articles that will be published in the journal. After a manuscript is technically edited and formatted, it will be removed from the “Just Accepted” Web site and published as an ASAP article. Note that technical editing may introduce minor changes to the manuscript text and/or graphics which could affect content, and all legal disclaimers and ethical guidelines that apply to the journal pertain. ACS cannot be held responsible for errors or consequences arising from the use of information contained in these “Just Accepted” manuscripts.



1
2
3 **Towards Understanding the Photocatalytic Activity of PbMoO₄ Powders with**
4
5 **Predominant (111), (100), (011), and (110) Facets. A Combined Experimental**
6
7 **and Theoretical Study**
8
9

10
11
12 **M.R.D. Bomio^{*,1}, R.L. Tranquilin², F.V. Motta¹, C.A. Paskocimas¹, R.M. Nascimento¹,**
13
14 **L. Gracia^{2,3}, J. Andres³ and E. Longo²**
15
16

17 ¹ LSQM- Laboratório de Síntese Química de Materiais - DEMat, Universidade Federal do Rio
18 Grande do Norte - UFRN, P.O. Box 1524, 59078-97, Natal, RN, Brazil T +558433422260
19

20
21 ² LIEC, Universidade Federal de São Carlos - UFSCar, P.O. Box 676, 13565-905, São Carlos,
22 SP, Brazil
23

24
25 ³ Departamento de Química Física y Analítica, Universitat Jaume I, 12071 Castello, Spain
26
27
28
29
30
31
32
33
34
35
36
37
38
39
40
41
42
43
44
45
46
47
48
49

50 *Corresponding author. Tel: +55-84-3342-2260; Fax: +55-84-3342-2406 E-mail address:
51 mauricio.bomio@ct.ufrn.br (M.R.D. Bomio).
52
53
54
55
56
57
58
59
60

Abstract

A complimentary combination of experimental work and first principle calculations, based on the Density Functional Theory (DFT) method, has been used to increase our limited understanding of the enhanced photocatalytic activity of PbMoO_4 powders with predominant (111), (100), (011), and (110) facets.

In this work, PbMoO_4 powders were prepared by the co-precipitation method and processed on a hydrothermal reactor at $100^\circ\text{C}/10$ minutes. The variation of different types of modifier such as acetylacetone (acac) or polyvinylpyrrolidone (PVP) is found to play a crucial role in controlling the particle size and morphology of products and their photocatalytic properties.

The structure and morphology of these crystals were characterized by X-ray diffraction (XRD), micro-Raman (MR) spectroscopy, field-emission gun scanning electron microscopy (FEG-SEM), and ultraviolet visible (UV-vis) absorption spectroscopy. Furthermore, the as-synthesized PbMoO_4 micro-octahedrons without presence of (001) surface exhibit enhanced activity for the photodegradation of rhodamine B (RhB) under ultraviolet-visible light irradiation.

Based on the theoretical and experimental results, we provide a complete assignment of the micro-Raman spectra of PbMoO_4 , while a growth mechanism for the formation of PbMoO_4 micro-octahedrons was systematically discussed, and a schematic illustration of the probable formation of morphologies in the whole of the synthetic process was also proposed, which reveals that the high photocatalytic activity is attributed to the absence of (001) facet.

Keywords: lead molybdates; hydrothermal syntheses; photocatalytic activity; Density Functional Theory (DFT) method

1. Introduction

Molybdates and tungstates-based oxides constitute important class of materials that exhibit various functional properties, in particular, metal molybdates have received special attention due to their novel and intriguing properties for widespread technological applications.¹⁻¹¹ Molybdates of relatively large bivalent cations (ionic radius > 0.99 Å: Ca, Ba, Pb, Sr) usually exist in the so-called scheelite structure form¹², and have attracted considerable interest due to their promising technological importance in a broad range of applications such as photoluminescence, scintillator materials, humidity sensors and catalysis¹³. As an important member of this family, lead molybdate (PbMoO₄) has gained increasing interest due to its use in a wide range of technological and theoretical fields^{12,14-24}, and experimental studies on the optical properties of lead molybdate have been published by different research groups.^{16,19,25-34}

PbMoO₄ crystallizes in tetragonal scheelite-structure having point group symmetry 4/m and space group I41/a, with two formula units per primitive cell.^{5,6}, and a specific feature of these systems is the existence of two different clusters into crystal lattice, in which each Mo is surrounded by four equivalent O atoms composing the [MoO₄]²⁻ tetrahedral configuration and each divalent metal, Pb, shares corners with eight adjacent O atoms, forming a [PbO₈]²⁻ configuration.

The research in materials science to development new properties and applications has been centered on the *bottom-up* approach. This technique is based on the construction of multifunctional nanostructures and devices by self-assembly of atoms and molecules.³⁵ The synthesis of micro and nanoscale inorganic materials with special morphology, size and hierarchy structure has attracted considerable attention in the past few decades due to their importance in basic scientific research and potential technological applications.^{36,37} Recently, the synthesis of metal molybdates has attracted attention due to their potential application in several fields.³⁸⁻⁴⁰ In particular, wet chemical synthesis (*bottom-up methods*) attracts great attention in the synthesis of PbMoO₄ crystals. The literature describes a range of approaches for synthesizing several molybdates, in particular lead molybdates, by different procedures, such as solid state

1
2
3 reaction^{41,42}, Czochralski crystal growth⁴³, chemical route⁴⁴, galvanic cell method⁴⁵, citrate
4
5 complex⁴⁶, sonochemical route^{47,48}, microemulsion method⁴⁹, microwave-assisted synthesis
6
7 method⁵⁰, precipitation method^{51,52}, solvothermal route¹² and hydrothermal method^{34,53,54}. In this
8
9 wide range of methods, in particular, the conventional hydrothermal (CH) method stands out
10
11 because it uses environmental friendly solvent, low processing temperatures and has reduced
12
13 cost.

14
15 PbMoO₄ presents excellent optical and chemical properties due to its electronic structure and
16
17 relatively low band gap energy as compared to above scheelite structures and may be a promising
18
19 photocatalyst. Therefore, it is of great importance to study the photocatalytic properties of this
20
21 material for potential applications. It is well-known that photocatalytic processes occur on the
22
23 surface of catalysts, and thus, size, shape and exposed crystal facets of crystals play a critical role
24
25 in the activity and efficiency of photocatalysts. The exposed facet of the PbMoO₄ crystal is an
26
27 important factor influencing its photocatalytic performance. The essence of exposed facets is the
28
29 surface atomic configuration and coordination, which show great effect on adsorption and
30
31 reactivity of semiconductor materials. In this context, Shen *et al.*⁵⁴ and Hashin⁵⁵ have proved that
32
33 PbMoO₄ microcrystals with preferentially exposed (001) facet exhibit higher catalytic activity
34
35 compared to that of (100) facet, enhancing the photocatalytic activity for degradation of
36
37 Rhodamine B (RhB) under light irradiation. Xing *et al.*⁵⁶ have obtained well-defined and uniform
38
39 PbMoO₄ polyhedral crystals via a microemulsion-based solvothermal method and the results of
40
41 RhB photocatalytic degradation showed that these PbMoO₄ polyhedrons display excellent
42
43 photocatalytic activity under visible ultraviolet light irradiation. Recently, Martínez de la Cruz *et*
44
45 *al.*^{57,58} successfully synthesized PbMoO₄ by a hydrothermal method in the absence of additives,
46
47 and its photocatalytic activity was tested under UV irradiation for the degradation reaction of
48
49 different organic dyes.

50
51 The aim of this work was to contribute to fill the gap between the single-crystal, powder and
52
53 microcrystalline worlds by comparing the surface properties of different facets of PbMoO₄,
54
55
56
57
58
59
60

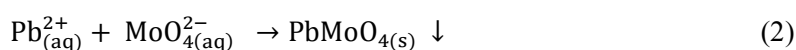
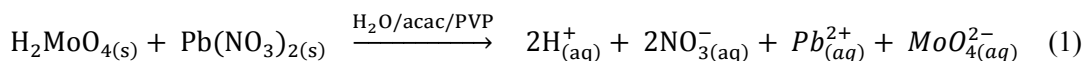
1
2
3 considered as models for mimicking the single-crystal world. Therefore, the validation of the
4 photocatalytic activity of PbMoO_4 and the effect of the different facets are the focus of this
5 contribution, in which new results on the synthesis of PbMoO_4 micro-octahedrons without the
6 presence of (001) facets were examined. We have now discovered, by investigating a set of
7 PbMoO_4 crystal facets with predominant (100), (110), (101), and (111) surfaces, present highest
8 photoreactivity. The materials were obtained by the co-precipitation method and processed by
9 hydrothermal method using two different modifiers at 100°C for 10 min. These micro-
10 octahedrons were analyzed by X-ray diffraction (XRD), micro-Raman (MR) spectroscopy,
11 ultraviolet visible (UV-vis) absorption spectroscopy and field-emission gun scanning electron
12 microscopy (FEG-SEM) and a micro-octahedrons growth mechanism is proposed and discussed
13 in detail. The photocatalytic activity of the material was evaluated for the degradation reactions of
14 rhodamine B (RhB). To complement these experimental measurements, the structural and
15 electronic properties of bulk ground and triplet PbMoO_4 were investigated, as well as the catalytic
16 activities of (001), (100), (110), (101) and (111) surfaces, using periodic density functional theory
17 (DFT) computations and a slab model, and an explanation of the photocatalytic activity of
18 PbMoO_4 powders without (001) facets is proposed. To our knowledge, this is the first report on
19 the preparation of PbMoO_4 with unique structure and on its photocatalytic properties.
20
21
22
23
24
25
26
27
28
29
30
31
32
33
34
35
36
37
38

39 **2. Experimental section**

40 **2.1 Synthesis of PbMoO_4 Crystals**

41 All chemicals used were analytical grade reagents without further purification, PbMoO_4 (PMO)
42 crystals were obtained by co-precipitation (CP) and hydrothermal methods in the presence of
43 acetylacetone (acac) (Vetec) as chelante modifier or polyvinylpyrrolidone (PVP) (Synth) as
44 coupling agent. The typical synthesis procedure is described as follows: 0.005 mol of molybdic
45 acid (H_2MoO_4) (Synth) and 0.005 mol of lead nitrate [$\text{Pb}(\text{NO}_3)_2$] (Merck) and such amount of
46 acac or PVP was dissolved in 75 mL of deionized water. Then, 5 mL of ammonium hydroxide
47 (NH_4OH) (30% in NH_3 , Synth) was added to the solution so that the pH value reached 11. These
48
49
50
51
52
53
54
55
56
57
58
59
60

suspensions were stirred for 10 min by ultrasound bath at room temperature. With this procedure, PMO crystals were obtained by the co-precipitation method. In a precipitation reaction, Pb^{2+} cations are electron pair acceptors (Lewis acids) while MoO_4^{2-} anions are electron pair donors (Lewis bases). The chemical reaction between these two species in solution results in the formation of PMO crystals as shown in the equations below:



These suspensions obtained were transferred into a stainless steel autoclave (lined with quartz glass), which was sealed and processed at 100°C for 10 min using heating rate fixed at 2°C/min. After hydrothermal processing, the autoclave was cooled down to room temperature. The resulting suspensions were washed several times with deionized water to neutralize the solution pH (≈ 7), and the white precipitates were dried with acetone and finally collected for characterization.

2.2 Characterization of $PbMoO_4$ Crystals

After hydrothermal processing at 100°C for 10 min, PMO crystals were structurally characterized by XRD using a Rigaku-DMax/2500PC (Japan) with Cu-K α radiation ($\lambda = 1.5406 \text{ \AA}$) in the 2θ range from 10° to 75° with scanning rate of 0.02°/s and total exposure time of 15 min. In addition, Rietveld routine was performed in the 2θ range from 10° to 110°, using an angular step of 0.02°/s and total exposure time of 90 min. In this work, the profiles of the XRD experimental patterns observed for the $PbMoO_4$ crystals were refined with a theoretical line profile known as Crystallographic Information File (CIF) with ID code 1011170.⁵⁹ Micro Raman measurements were recorded using a T-64000 spectrometer (Jobin-Yvon, France) triple monochromator coupled to a CCD detector at 488 nm wavelength of an argon ion laser. Its maximum output power was kept at 10 mW with the use of lens (100 μm) to prevent sample overheating. The morphologies

1
2
3 were investigated using FEG-SEM (Carl Zeiss, model Supra 35-VP, Germany) operated at 6 kV.
4
5 UV-vis spectra were taken using a Varian spectrophotometer, model Cary 5G (USA) in diffuse
6
7 reflection mode with MgO as standard.
8

9 10 **2.3 Photocatalytic activity measurement**

11 The photocatalytic properties of PMO crystals (as a catalyst agent) for the degradation of
12 Rhodamine B (RhB) dye with molecular formula $[C_{28}H_{31}ClN_2O_3]$ (99.5% purity, Mallinckrodt) in
13 an aqueous solution were tested under UV-light illumination. About 50 mg catalyst crystals were
14 placed in a 250 mL beaker, being added of 50 mL RhB solution (1×10^{-5} mol L⁻¹) pH 4. These
15 suspensions were ultrasonicated for 10 min in ultrasonic cleaner before illumination then stored
16 in the dark for 5 min to allow the saturated absorption of RhB onto the catalyst. The beakers were
17 then placed in a photo-reactor at 20 μ C and illuminated by six UV lamps (TUV Philips, 15 W,
18 with maximum intensity at 254 nm). The power light was measured by Coherent Power Max
19 model No PM10 and the optical energy density value was 20 mW cm⁻². At two-minute intervals,
20 one 3 mL aliquot of these suspensions was removed and centrifuged at 9000 rpm for 5 min to
21 remove crystals in suspension. Finally, variations of the maximum absorption band of supernatant
22 solutions were monitored by UV-vis absorbance spectra measurements using a double-beam
23 spectrophotometer with double monochromator and a JASCO photomultiplier tube detector
24 (Model V-660, USA).
25
26
27
28
29
30
31
32
33
34
35
36
37
38
39
40

41 **3. Computational section**

42 **3.1 Bulk**

43
44 Calculations for PbMoO₄ were performed using the CRYSTAL09⁸⁰ software package. Lead atom
45 has been described by a Hay-Wadt pseudo-potential scheme with large core, HAYWLC-2111dG;
46 molybdenum and oxygen centers by 976-6311d31G and 6-31d1G basis set, respectively, which
47 was taken from the Crystal web site.⁸¹ Becke's three-parameter hybrid non-local exchange
48 functional⁸² combined with a Lee-Yang-Parr gradient-corrected correlation functional (B3LYP)⁸³
49 was used. Diagonalization of the Fock matrix was performed at adequate *k*-point grids in the
50
51
52
53
54
55
56
57
58
59
60

1
2
3 reciprocal space. The thresholds controlling the accuracy of the Coulomb calculation and
4
5 exchange integrals were set to 10^{-8} (ITOL1 to ITOL4) and 10^{-14} (ITOL5), whereas the percentage
6
7 of Fock/Kohn-Sham mixing matrices was set to 40.⁸⁰ Full optimization of scheelite-type PbMoO_4
8
9 cell parameters (a and c) and internal atomic position for the bulk PbMoO_4 were carried out.

11 **3.2 Surface energy**

12
13 Surface energy is one of the key factors controlling the number of active sites and, accordingly,
14
15 the photocatalytic activity of PbMoO_4 . The low-index (001), (100), (110), (101) and (111)
16
17 surfaces were modeled by unreconstructed (truncated bulk) slab models by using calculated
18
19 equilibrium geometry. Because these surfaces have different number of atoms in each layer to
20
21 reach symmetry and stoichiometry, the low-index surfaces were modeled with different
22
23 thicknesses in the z -direction but were periodic in the x - and y -directions. After the corresponding
24
25 convergence test on the systems, slab models containing 15, 20, 15, 15, 12 and 50 atomic layers
26
27 for the (001), (100), (110), (101) and (111) surfaces, respectively, were selected. For the models
28
29 used here, bottom and top planes were equivalent in symmetry. A complete relaxation in each
30
31 model was performed.
32
33

34 **3.3 Wulff construction**

35
36
37 Gibbs defines⁶⁰ equilibrium morphology as the minimum energy conformation of faces of a
38
39 fixed-volume crystal, which can be directly identified from the Wulff construction⁶¹ on the polar
40
41 plots of surface energies. It could be inferred that the faceted geometry of crystals is due to the
42
43 existence of a finite number of minima in polar plots⁶². The theoretical equilibrium shape of a
44
45 crystal is unique since, at a given temperature and pressure, it only depends on one
46
47 thermodynamic property, *i.e.* on the ratio between specific surface energies (χ_{hkl}) of different
48
49 forms. Hence, predicting the equilibrium of a crystal can be reduced to calculating the χ_{hkl} values
50
51 without the presence of foreign adsorption (solvent and/or impurities), and the Wulff
52
53 construction⁶¹ is a standard method for determining the equilibrium shape of bulk crystals. The
54
55 underlying basis for these size- and shape- dependent thermodynamic constructions states that the
56
57
58
59
60

1
2
3 equilibrium shape of macroscopic crystals can be found by minimizing the surface energies with
4 respect to a fixed volume as discussed in detail by Herring.⁶³ The energy of the terminated
5 surface of a solid material is always higher than the bulk energy, and this energy difference is
6 defined as the surface energy. Based on surface energies of all facets, the Wulff construction can
7 be used to determine the equilibrium morphology of a material. Surface energy minimization is
8 the central standard to optimize the composition of the crystal surface. The surface relative
9 energy variations can basically be explained by the different chemical compositions of facets,
10 which result in diverse degrees of broken chemical bonds on their surface⁶⁴⁻⁶⁶ and sites. The
11 shorter and stronger bonds in the surface skin (up to two or three atomic layers) dominate the size
12 dependency while bonds in the interior core remain in their bulk nature. Wulff construction^{61,67}
13 was applied to build theoretical crystals by using the *ab initio* calculated surface energies and the
14 PbMoO₄ *I*4₁/*a* crystal structure. The surface energy, *E*_{surf}, is defined as the total energy per
15 repeating cell of the slab minus the total energy of the same number of atoms of the perfect
16 crystal divided by the surface area per repeating cell of the two sides of the slab, *i.e.* *E*_{surf} =
17 $(E_{\text{slab}} - n E_{\text{bulk}}) / 2A$. This equation has been used by us in previous studies.^{31,68,69}
18
19
20
21
22
23
24
25
26
27
28
29
30
31
32
33
34
35
36

37 **3.4 Excited states**

38
39 Information on the excited states in tungstates and molybdates is deeply desired to understand the
40 de-excitation processes after high-energy electronic excitation, since these materials are widely
41 used for scintillation detectors. Density functional theory (DFT) and its extensions have been
42 used to understand the role of the electronic excited states in the PL behaviour observed in
43 scheelite-³³ and perovskite-based materials⁷⁰, a fundamental issue that remains far from being
44 fully understood. Based on the molecular orbital theory, Itoh and Kajitani⁷¹ have recently
45 reported that the intrinsic luminescence bands of PbMoO₄ originate from the radiative transitions
46 from the triplet ³T₁ and/ or ³T₂ states to the ¹A₁ ground-state and that the symmetry lowering of
47 (MoO₄)⁻² ions from T_d to C_{3v} due to the Jahn-Teller effect could lift the degeneracy of the ³T₁ and
48
49
50
51
52
53
54
55
56
57
58
59
60

³T₂ states. The presence of excited electronic states and how they can be associated to in-gap defect states give rise to PL emissions. In addition, our investigations of different excited facets of PbMoO₄ may be helpful to comprehend the photoreactivity and catalytic activity of PbMoO₄. To find the excited triplet electronic state, an initial dislocation from the ground state has been made in order to induce deformation on one [MoO₄] cluster to a trigonal pyramid.⁷¹ Then, a full optimization is performed. Vibrational analysis has been made to ensure that there are no imaginary frequencies and the structure corresponds to a minimum for the ground and excited triplet states. The band structures have been obtained along the appropriate high-symmetry paths of the Brillouin zone. Finally, the low-index (001), (100), (110), (101) and (111) surfaces were modeled at triplet state using the optimized geometry of the bulk in excited triplet state.

4. Results and discussion

4.1 X-ray diffraction and Rietveld Analysis

X-ray patterns of PMO/acac and PMO/PVP powders processed in hydrothermal system at 100°C for 10 min are presented in Figure 1. XRD patterns revealed that all diffraction peaks of PMO/acac and PMO/PVP micro-octahedrons can be indexed to the scheelite-type tetragonal structure without the presence of secondary phases, in agreement with the respective Joint Committee on Powder Diffraction Standards (JCPDS) card n^o. 44-1486.⁷² Moreover, the relative intensities and sharp diffraction of all peaks indicated that the materials are well-crystallized, suggesting an ordered structure at long range.

Insert Figure 1

In order to deeply investigate the small differences in the structure of materials, the lattice parameters and the unit cell volume of materials were calculated using the Maud software version 2.26.^{73,74} The results obtained from the Rietveld refinement for lattice parameters and cell volumes are shown in Support information, Figure SI-1 and shown in Table 1.

Insert Table 1

As can be seen in Table 1, the PMO/acac and PMO/PVP unit cell parameters obtained by Rietveld refinement indicate a good agreement to those reported in literature.^{17,21} Moreover, it is possible to observe a slight distortion on the PMO/acac and PMO/PVP structures processed by hydrothermal method at 100°C/10 min, especially in the *c* parameter of the PMO/acac system, which can be related to synthesis reactants, *i.e.* influence of distinct organic composition of modifiers and the experimental hydrothermal conditions adopted. In addition, the distortion of the PMO/acac system can be assigned to the presence of solvent molecule and/or OH group from the acetylacetone trapped into the crystal lattice.

4.2 Micro-Raman Spectroscopy

The group theory calculation presents 26 different vibrations for the PbMoO₄, which can be represented by equation 3^{75,76}, where all vibrations A_g, B_g, and E_g are Raman active.

$$\Gamma = 3A_g + 5A_u + 5B_g + 3B_u + 5E_g + 5E_u \quad (3)$$

In materials with scheelite-type structure, the first member of the pairs (g) is a Raman-active mode and the second member (u) is active only in infrared (IR) frequencies, except for B_u silent modes that are not IR-active. Consequently, 13 zone-center Raman-active modes are expected in PbMoO₄, as described by equation 4⁷⁷.

$$\Gamma = 3A_g + 5B_g + 5E_g \quad (4)$$

Figure 2 ((a) PMO/acac and (b) PMO/PVP) shows the Raman spectra in the range from 50 to 1000 cm⁻¹ of PbMoO₄ samples processed by hydrothermal method at 100°C/10 min with acetylacetone and polyvinylpyrrolidone, respectively.

According to literature⁷⁸, it was possible to observe two characteristic vibration groups for molybdate materials. The first vibration mode corresponds to external vibrations, which are related to lattice phonons from the [PbO₈] clusters in fixed cells units. The second belongs to internal vibrations related to [MoO₄] cluster in the lattice, which are composed of four Raman-active internal modes, *v*₁ (A₁), *v*₂ (E₁), *v*₃ (F₂) and *v*₄ (F₂), one free rotation mode *v*_{fr.} (F₁) and one translational mode (F₂). As can be seen in Figure 2, the results indicated that all Raman-active

1
2
3 modes of PMO/acac (a) and PMO/PVP (b) obtained by hydrothermal method in this work are
4
5 characteristic of a tetragonal structure, in agreement with data previously reported in literature
6
7 ^{25,34,59,79,80}. Moreover, the well-defined active-Raman modes suggest that PbMoO₄ are structurally
8
9 ordered at short-range, regardless of the different types of modifiers used during hydrothermal
10
11 synthesis.
12

13 *Insert Figure 2*

14
15
16 Theoretical Raman modes are shown in the low part of Figure 2. They are in agreement
17
18 with experimental values up to 200 cm⁻¹. The modes can be organized in two groups. One group
19
20 is composed of low-frequency modes with frequencies smaller than 357 cm⁻¹, associated to
21
22 internal bending movements of the MoO₄ tetrahedra. The second group is separated from the first
23
24 group by a phonon gap of about 400 cm⁻¹, and is formed by the last three modes associated to
25
26 Mo-O stretching movements. In relation to experimental Raman modes, there are some
27
28 differences between these data and those previous published ⁸¹. B_g modes (70 and 197 cm⁻¹) now
29
30 appear at ~170 and ~330 cm⁻¹, and the A_g mode at 324 cm⁻¹ disappears.
31
32

33
34 First principle calculations indicate loss of symmetry in achieving the triplet state of
35
36 PbMoO₄ generating a structure with parameters a = 5.326 Å, b = 5.332 Å, c = 5.332 Å and angles
37
38 $\alpha = 90.018^\circ$, $\beta = 90.004^\circ$, $\gamma = 90.021^\circ$. In the triplet state, a distortion in the surroundings of
39
40 [MoO₄] and [PbO₈] clusters compared to the fundamental state was observed. One [MoO₄] unit
41
42 maintains the Mo-O distances at 1.801 Å and angles at 107.4° and 113.8°, while the other
43
44 increases its value at 1.876 Å and also the distortion with angles of 103.4° and 122.2°. In crystals
45
46 with the scheelite structure, the indicator of distortion in the surroundings of the tetrahedral anion
47
48 is the high-frequency A_g vibration, which is the result of the Davydov splitting of the (A₁)v₁ free
49
50 tetrahedral anion.^{82,83} The A_g mode in the fundamental s state is 314.3 cm⁻¹. In passing from s to t*
51
52 state, the A_g mode increases to 360.1 cm⁻¹. [PbO₈] clusters are also modified, passing to excited
53
54 state. Four Pb-O distances of 2.627 Å and other four of 2.639 Å evolve to more distorted clusters
55
56 with Pb-O distances of 2.519-2.636 Å in one [PbO₈] unit and 2.358-2.598 Å in the other [PbO₈],
57
58
59
60

1
2
3 which form the unit cell. B_g modes in fundamental state (309.1 cm^{-1}) involve Mo-O-Pb motion,
4
5 which can favour the distortion of $[\text{PbO}_8]$ clusters in t^* state (307.4 cm^{-1}).
6
7

8 **4.3. FEG-SEM analysis**

9
10 Figures 3(a-b) and 3(c-d) show the FEG-SEM images for the PMO/acac and PMO/PVP micro-
11
12 octahedrons, respectively. As can be seen, the presences of modifiers, acetylacetone and
13
14 polyvinylpyrrolidone have a significant influence on the morphology of lead molybdate powders.
15

16 **Insert Figure 3**

17
18 However, Figure 3 (a) shows the FEG-SEM image of PMO/acac processed at $100^\circ\text{C}/10\text{ min}$. A
19
20 wide homogeneity between micro octahedrons with well-defined superficial morphology of the
21
22 material was observed. On the other hand, due to the presence of acetylacetone during the
23
24 hydrothermal processing, the micro-octahedrons exhibit interesting morphology (Fig. 3b). In
25
26 contrast to a PMO crystal simulated by using the Java Structure Viewer Program^{84,85}, and
27
28 according to a previous work³⁴, it was found that the growth of the crystallographic plane (001)
29
30 is not favored in the presence of acetylacetone chelate modifier.
31
32

33
34 In principle, few works in literature have reported that acetylacetone is widely used as a chelating
35
36 agent to form ligands with metal ions⁸⁶, stabilizer of ZnO nanoparticles in water as
37
38 functionalizing agent⁸⁷, solvent for solvothermal syntheses of spherical ZrO_2 ⁸⁸ and as modifier
39
40 for perovskite thin film⁸⁹. We believe that the formation of a complex between the lead ions and
41
42 acetylacetone during the hydrothermal synthesis does not favor the growth of the crystallographic
43
44 plane (001). This mechanism will be discussed later.
45

46
47 Figure 3 (c) shows the FEG-SEM image of PMO/PVP processed at $100^\circ\text{C}/10\text{ min}$. In these
48
49 conditions, surface defects on micro-octahedrons facets are observed, and the coalescence process
50
51 of the material contributed to the growth of several micro octahedrons and resulted in a
52
53 imperfectly oriented attachment mechanism^{90,91} between particles, where a crystal growth along
54
55 $[001]$ is preferred than on the $[100]$ direction.^{92,93}
56
57
58
59
60

1
2
3 Nevertheless, FEG-SEM micrographs were also used to estimate the average particle size
4 distribution of PMO/acac and PMO/PVP micro-octahedrons. The average particle size
5 distribution for micro-octahedrons synthesized by hydrothermal conditions at 100°C/10min
6 shows the average particle height of 0.74 μm and average particle width of 0.60 μm for the
7 PMO/acac system and 0.55 μm average particle height and average particle width of 0.48 μm for
8 the PMO/PVP system (see additional information in figure SI-2).
9

10
11
12 With the use of PVP during the synthesis of PMO micro-octahedrons, the coupling agent
13 promotes the oriented attachment mechanism growth, as shown in Figure 3(c,d). However, the
14 average particle size of PMO/PVP is smaller than that of PMO/acac. This difference on particles
15 sizes arise from the PVP molecules adsorbed onto all PMO surface during the reaction makes the
16 controllable nucleation and growth of particles, having as a consequence lower average particles
17 size of PMO.
18
19

20
21 Compared to PMO/acac micro-octahedrons, the lead acetylacetonate complex does not favor the
22 oriented attachment mechanism or the crystallographic plane (001) as shown in Figure 3(a,b), but
23 micro-octahedrons can grow in the other crystallographic direction due to the absence of lead
24 acetylacetonate complex in these directions.
25
26

27 28 29 30 31 32 33 34 35 36 37 **4.4. Growth mechanism**

38
39 Figure 4 illustrates a possible growth mechanism by the effect of acetylacetone and
40 polyvinylpyrrolidone on the shape of micro-octahedral and particle size growth. The growth
41 mechanism will be suggested by the influence of the modifiers on the syntheses of different
42 materials reported in literature, supported on FEG-SEM micrograph observations.
43
44
45
46

47 48 ***Insert Figure 4***

49
50 Firstly, by adding the lead nitrate in contact with molybdic acid in aqueous solution without the
51 presence of any modifier, both ions are free to move in the solution. One can formally consider
52 the coordination sphere of the water in both ions Pb^{2+} and MoO_4^{-2} are present which causes a fast
53 dissociation of the chemical salts in solution. The positive and negative partial charges of the H_2O
54
55
56
57
58
59
60

1
2
3 are responsible to surround the ions, maintained as close as possible to each other (Figure 4a).

4
5 However, due to differences in the electronic density between Pb^{2+} and MoO_4^{2-} ions, a strong
6
7 electrostatic attraction force occurs between both, resulting in the formation of the first $\text{PbMoO}_{4(s)}$
8
9 precipitate. Secondly, the precipitation rate increased by the addition of 5 mL of NH_4OH (pH=11)
10
11 into this solution. When one of these suspensions was processed by hydrothermal condition, it is
12
13 possible to note an increase in the PbMoO_4 crystal size and also to detect all facets of the micro-
14
15 octahedral particles, including the 001 face, as reported in a previous work.³⁴
16
17

18 In the case of acetylacetone, there is a tautomeric equilibrium between keto and enol forms in
19
20 solution, where the keto shape is in equilibrium with the cyclic enol form. The acetylacetone
21
22 behaves mainly as a bidentate O^- donor ligand forming six-membered chelates with numerous
23
24 metal ions, including Pb^{2+} ion (Figure 4 (b)).
25
26

27 When acetylacetone is added to the reaction medium, it behaves like a weak acid. The anion
28
29 resulting from this ionization, acetylacetonate can act as a ligand for metal ions. The coordination
30
31 of the deprotonated enol form, the acetylacetonate ion (accac^-) to metal cations usually results in
32
33 neutral complexes, which in the case of Pb^{+2} , results in a complex with square pyramid geometry
34
35 ($\text{Pb}(\text{accac})_2$). We believe that, the complex geometry of ($\text{Pb}(\text{accac})_2$) significantly contributed to
36
37 the evolution of the new morphology observed for the synthesis of PMO/acac powders. The
38
39 complex played a role in the inactivation through a steric layer, which is the case of the
40
41 acetylacetonate structure (Figure 4 (c)), which in turn has favored inhibition of the specific
42
43 crystallographic plane [001] (Figure 4 (d)) at the time of nucleation and formation of PbMoO_4
44
45 micro-octahedra, during the hydrothermal process at $100^\circ\text{C}/10\text{min}$ (Figure 4 (m)).
46
47

48 On the other hand, the use of polyvinylpyrrolidone coupling agent to control the morphology of
49
50 the PbMoO_4 also observed it was revealed morphological changes of the material.
51
52 Polyvinylpyrrolidone is extensively used as the stabilizer and structure-directing agent in
53
54 nanotechnology due to its excellent adsorption ability and solubility in water.
55
56
57
58
59
60

1
2
3 In the case of PVP, its presence during the reaction promoted an increase in the viscosity of the
4 reaction medium, which plays the role of decreasing the spontaneous interaction between Pb^{+2}
5 and MoO_4^{-2} ions, even under hydrothermal processing conditions for 10 minutes at 100°C (Figure
6 30 (e)). We believe that as a consequence of the use of polyvinylpyrrolidone, a slow rate of
7 formation (nucleation) and aggregation of several microcrystals take place in the system,
8 promoting the formation of the PbMoO_4 micro-octahedra (Figure 4 (f)) by coalescence, which
9 contributes to the growth of distorted and disordered micro-octahedra by growth mechanism of a
10 crystallographic orientation mechanism (Oriented Attachment) (Figure. 4 (g)) and additional
11 information in figure SI-3).

22 ***Surfaces and growth mechanism***

23
24
25 Since many types of metal oxides form a wide range of oxygen-deficient intermediate phases,⁹⁵⁻⁹⁷
26 it is generally believed that the reconstruction of the metal oxide surface is related to an ordered
27 oxygen vacancy type defect.^{97,98} The analysis of different Pb and Mo arrangements in different
28 planes leads to diverse degrees of broken chemical bonds on their surface and sites. While bonds
29 and coordination in the core interior remain their bulk nature, i.e. MoO_4 and PbO_8 , in the surface
30 undercoordinated Pb is found. The electronic structure of PbMoO_4 surfaces has scarcely been
31 studied. Table 2 presents the calculated surface energy values (E_{surf}) for (001), (100), (110),
32 (101) and (111) facets, the number of PbMoO_4 layers of each surface model and their calculated
33 band gap energy. Figure 5 shows the resulting geometry of optimized surfaces.

45 **Insert Table 2**

47 **Insert Figure 5**

49 In the (001) surface, Pb is surrounded by six O atoms, three sets of two equivalent distances 2.43,
50 2.50 and 2.72 Å, respectively. The (100) surface shows a Pb coordinated to five O atoms at
51 distances 2.23 (x2), 2.31, 2.89 and 2.92 Å, respectively. In the (110) and (111) surfaces, Pb is
52 surrounded by only four O atoms at a range of distances 2.17-2.87 Å, and 2.26-2.92 Å,
53 respectively. Mo atoms have a tetrahedral environment in all surfaces more distorted than in bulk,
54
55
56
57
58
59
60

1
2
3 with clearly two different distances, 1.75 and 1.86 Å in (001); 1.71 and 1.79 Å in (100); 1.74 and
4
5 1.87 Å in (110), respectively. Therefore, undercoordination at Pb atom can explain the stability
6
7 order of surface energy between surfaces, since the lack of three or four O atoms in (100) or (110)
8
9 and (111) facets, respectively, induces more distortions than the deficiency of two O atoms in
10
11 (001) facets.³² In the case of (101) facet, Pb atoms are located far from the top of the surface and
12
13 are coordinated to six O atoms (in the range 2.32-2.94 Å). Figure 6 shows the resulting Wulff
14
15 construction derived from calculated surface energy values⁹⁴ for different crystalline planes.
16
17 Although theoretical calculations predict a low percentage of (100) and (110) facets in the
18
19 resulting morphology, both experimental and theoretical results point out that a crystal growth
20
21 along [001] crystal direction is preferred to the [100] direction for PbMoO₄. A growth
22
23 combination along the [001] direction may lead to the formation of octahedron-like PbMoO₄
24
25 microcrystals with small exposed (001) facets at the top and bottom of the octahedron-like
26
27 microcrystals.³⁴
28
29

30 **Insert Figure 6**

31
32 The second surface in order of stability is (100) (see Table 2), and therefore it appears in
33
34 the Wulff construction (Figure 6) obtained from the computed surface energies. Although the
35
36 (100) surface is not experimentally seen, it has a small extent in equilibrium morphologies
37
38 reported in literature.⁹⁵
39

40 **4.5. UV-vis absorption spectroscopy analyses**

41
42 The UV-vis absorbance spectra of PMO/acac and PMO/PVP micro-octahedrons synthesized at
43
44 100°C for 10 min was used to understand how the hydrothermal processing can introduces
45
46 intermediates energy levels within the band gap of these materials. Wood and Tauc⁹⁶ proposed a
47
48 method to estimate the optical band gap energy (E_{gap}), which is associated with absorbance and
49
50 photon energy by the following equation.
51
52

$$53 \quad hv\alpha \propto (hv - E_{gap})^n \quad (3)$$

54
55
56
57
58
59
60

1
2
3 where α is the absorbance, h is the Planck constant, ν is the frequency, E_{gap} is the optical band
4 gap, and n is a constant associated with the different types of electronic transitions ($n= 1/2, 2, 3/2,$
5 or 3 for direct allowed, indirect allowed, direct forbidden, and indirect forbidden transitions,
6 respectively). According to Lacomba-Perales⁹⁷ *et al* and previous report³⁴, molybdates with
7 scheelite-type tetragonal structure present direct allowed electronic transition, *i.e.* n equal to 1/2.
8 The band gap was estimated using equation 3, and the results obtained are listed in Table 3,
9 which can be compared with E_{gap} values recently reported in literature. Our research group
10 synthesized the hierarchical assembly of CaMoO_4 nano-octahedrons and their photoluminescence
11 properties and structural order-disorder effect as a function of the particle/region size⁹⁸ have been
12 studied. This work analyzes the structure order-disorder using theoretical models and concludes
13 that geometric distortions along the y and z planes of the scheelite structure affect the order-
14 disorder in the lattice, which causes the appearance of intermediate energy levels within the band
15 gap.

16
17
18
19
20
21
22
23
24
25
26
27
28
29
30
31 In Figure SI-4, the PMO/acac and PMO/PVP band gap values were 3.05 eV and 3.17 eV,
32 respectively. We can observe the result of refinement Rietveld method (Table 1) that the structure
33 parameter of PMO/PVP are closer to the reference used in the work (JCPDS 44-1486) than
34 PMO/acac. Therefore, the increase in structural organization leads to a reduction in these
35 intermediary energy levels, increasing the E_{gap} values. The presence of disorder structure of
36 PMO/acac due to increased defects in the lattice (tetrahedral and octahedral distortion) favors the
37 decrease in the bad gap, which can be directly related to increased defects, such as absence of
38 (001) face on the micro-octahedron morphology (Figure 3d), which raises the local levels within
39 the band gap region, reducing the optical band gap measure.

4.6. Photocatalytic activity of PbMoO_4

40
41
42
43
44
45
46
47
48
49
50
51
52 Recently, several studies have investigated the photocatalytic degradation properties of PbMoO_4
53 of different types of organic dyes. For this purpose, different synthesis routes have been proposed
54
55
56
57
58
59
60

1
2
3 to obtain new structural morphologies and particle size, in order to improve the photocatalytic
4 properties^{55-57,99-101}
5
6

7
8 In this work, with the aid of different modifiers, it was possible to modify the morphology and
9 creates defects on the surface and PbMoO₄ clusters, as can be seen in Figures 3b and 3d. In order
10 to demonstrate the photocatalytic activity of PMO/acac and PMO/PVP materials obtained by
11 hydrothermal synthesis at 100°C/10min, photodegradation of RhB dye was carried out in aqueous
12 dispersion (RhB + PMO/acac or PMO/PVP) under UV lamps with maximum intensity at 254 nm.
13
14 The temporal evolution of adsorption and photocatalytic degradation of aqueous RhB dye
15 solution (C_n/C_0) is shown in Figure 7. To observe the influence of acetylacetone and
16 polyvinylpyrrolidone on the PbMoO₄ micro-octahedrons morphology, similar experiment for
17 PbMoO₄ micro-octahedrons without any modifier addition (PMO/WS) was carried out. The
18 structural, morphological and optical characterization of these micro-octahedrons can be seen in
19 our previous work.³⁴ As can be seen in Figure 7 (a), for PMO/WS micro-octahedrons, the RhB
20 dye was totally photodegraded after 55 min under UV light illumination. The result indicates that
21 even without any modification on the PbMoO₄ morphology, the RhB photodegradation efficiency
22 is high. On the other hand, for the synthesized PMO/acac and PMO/ PVP materials (Figure 7 (b)
23 and (c), respectively, the photodegradation rate of RhB dye was higher than PMO/WS due to the
24 action of modifiers, which promoted remarkable changes on the PbMoO₄ morphology, having as
25 consequence the formation of surface defects and distortions in [MoO₄] or [PbO₈] clusters. The
26 degradation degree of the RhB dye increases when PbMoO₄ was synthesized by hydrothermal
27 process at 100°C/10min with polyvinylpyrrolidone coupling agent (Figure 7 (c), where the RhB
28 dye was totally photodegraded after 45 min under UV light illumination. According to literature,
29 scheelite-type structure tend to be faceted and aligned by “docking” processes involving
30 crystallographic fusion between some faces with lower surface energy because they are more
31 abundant and generate an extended morphology.³¹ Figure 3 (c) and Figure SI-3 (c,d) show the
32 growth process of these morphologies through a self-organization of adjacent microcrystals in a
33
34
35
36
37
38
39
40
41
42
43
44
45
46
47
48
49
50
51
52
53
54
55
56
57
58
59
60

1
2
3 similar crystallographic orientation (“oriented attachment”). The growth along the [001]
4
5 direction, promoted the aggregation of several particles on similar crystallographic orientations,
6
7 favoring the coalescence of PbMoO₄ micro-octahedrons, which promote more potential active
8
9 sites on the surface (defects), in relation to PMO/WS for RhB dye photodegradation.

10
11 For PMO/acac materials, different morphologies compared to PMO/WS and PMO/PVP were
12
13 observed. Recently, Shen *et. al.*,⁵⁴ synthesized PbMoO₄ microcrystals with preferentially exposed
14
15 (001) facets by a facile surfactant-assisted hydrothermal process in the presence of
16
17 cetyltrimethylammonium bromide (CTAB), which exhibited higher catalytic activity compared to
18
19 (110) facet. Similarly, Hashim *et. al.*,⁵⁵ produced PbMoO₄ dendrites with exposed on (001) facet
20
21 with photocatalytic thorough the degradation of rhodamine B.
22
23

24
25 In our work, it was observed that the absence of the (001) facet exhibited enhanced activity for
26
27 the RhB photodegradation instead of exposing it. As can be seen in Figure 7 (b), the complete
28
29 degradation of the RhB dye was achieved in only 14 min of exposure to UV light, demonstrating
30
31 the high catalytic properties of PbMoO₄ in the absence of the (001) face in the material structure,
32
33 as shown in Figure 3 (b). In our research group, a model based on complex clusters was proposed
34
35 to explain the photocatalytic activity of SrWO₄ microcrystal due to the photo-oxidation of RhB
36
37 ¹⁰². For PbMoO₄ synthesized by hydrothermal method at 100°C/10 min with acetylacetone, we
38
39 believe that PbMoO₄ catalyst without the presence of (001) facet has higher ability to generate e⁻
40
41 h[•] pairs due to defects on the specific surface (001), providing a fast degradation of the RhB dye.
42
43
44

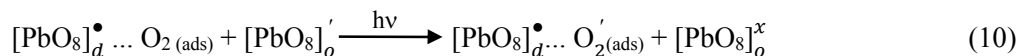
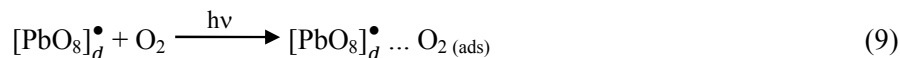
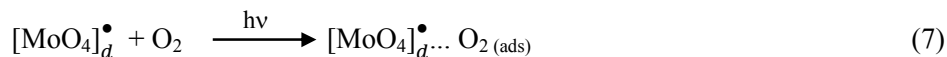
45 The cluster-like elucidation of the photocatalytic performance is supported and strengthened by
46
47 different extrinsic (surface) and intrinsic (bulk) defect distribution. The defect structure and
48
49 density variation surface and/or bulk might be responsible for the different photocatalytic
50
51 behavior of PbMoO₄. Effective charge separation (electron/hole) requires the presence of a
52
53 cluster-to-cluster charge transfer (CCCT) of electrons or holes from [MoO₄]_o^x / [MoO₄]_d^x or
54
55 [PbO₈]_o^x / [PbO₈]_d^x. One way to boost photocatalyst efficiency is to exchange ordered complex
56
57
58
59
60

clusters to disordered complex clusters. Consequently, the effect of surface properties on the photocatalytic performance should be considered in terms of $[\text{MoO}_4]_o^x$, $[\text{PbO}_8]_o^x$ clusters and $[\text{MoO}_4]_d^x$, $[\text{PbO}_8]_d^x$ clusters, where o = order and d= disorder.

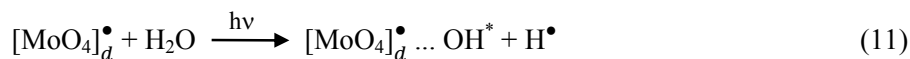
The first effect is intrinsic to the PbMoO_4 material and is derived from the bulk/surface material composed of an asymmetric distorted $[\text{MoO}_4]_d$ or $[\text{PbO}_8]_d$ and ordered $[\text{MoO}_4]_o$ or $[\text{PbO}_8]_o$. The ordered complex cluster often behaves as electrons sink and improve the charge separations within the semiconductor photocatalytic system. These electron polarons can then be discharged to acceptors (O_2) at the interface with a relatively lower over reduction potential. Consequently, the effect of surface properties on the photocatalytic activity should be considered in term of the following reactions:



Upon the adsorption of a photon with energy equal to or greater than the band gap of the semiconductor, an electron polaron/hole pair is generated in the bulk/surface. These charge carriers migrate toward the catalytic surface where the charge transfer between the perfect or defective surface and adsorbed oxygen molecules produces several kinds of charged species including O_2' superoxide ion. The molecular oxygen reactivity with $[\text{MoO}_4]$ or $[\text{PbO}_8]$ results in the following species:



The clusters formed by the complex PbMoO_4 cluster interact with water and separate it into its hydroxyl radicals and hydrogen ions according to following reactions:



The primary products of the partial oxidation reaction between water and a complex cluster $[\text{MoO}_4]_d^\bullet$ or $[\text{PbO}_8]_d^\bullet$ are hydroxyl radicals, OH^\bullet . These radicals exhibit high oxidation power and produce mineralization of an organic compound in water. The primary reaction is the formation of superoxide species $[\text{MoO}_4]_d^\bullet \dots \text{O}'_2$ or $[\text{PbO}_8]_d^\bullet \dots \text{O}'_2$. These species then react with hydrogen ion H^\bullet and form a hydrogen peroxide radical ($\text{O}_2\text{H}^\bullet$) according to the following reactions:



OH^\bullet and $\text{O}_2\text{H}^\bullet$ radicals react with an organic compound and ultimately cause their oxidation. The nature of superoxide radicals can be described using a complex cluster where the polaron/hole polaron electron exchanges from structural disorder to structural order to absorb molecular oxygen and water molecular oxygen and water.

Finally, it is noteworthy that it is still challenging to correlate the surface defects with the photocatalytic activity. A major problem is that the defects are interacting with many other factors and the photocatalytic activity of PbMoO_4 can be dominated by the balance between all these factors. One should keep in mind that defects exist in most PbMoO_4 samples except perfect single crystals, and the degrees of defects may differ greatly in different samples. Therefore, it is almost impossible to exclude the effects of defects on the photocatalytic activity of PbMoO_4 when studying the effects from other factors, e.g. crystalline phases and exposed crystal facets, while it is rational to investigate the sole effect of defects on the photocatalytic activity of PbMoO_4 , providing that other factors could be kept unchanged.

4.6. Electronic structure of bulk ground and triplet states, and surfaces

Figure 8(a) shows the band structure and DOS projected on atoms for the triplet structure. The distortion process on the fundamental $[\text{MoO}_4]_d$ and $[\text{PbO}_8]_d$ clusters to the excited $[\text{MoO}_4]_d^\bullet$

1
2
3 and $[\text{PbO}_8]_d^*$ tetrahedral and deltahedral groups, respectively, favour the formation of
4 intermediary energy levels in the conduction band (CB) conferring conductor properties to this
5 material. In the ground state, the top of the valence band (VB) is located on the Δ point and the
6 bottom of the conduction band (CB) is on point N, presenting an indirect band gap of 3.69 eV.⁸¹
7
8 Zhang *et al.* investigated in detail the electronic band structures of crystalline PbWO_4 , PbMoO_4
9 CaWO_4 , and CaMoO_4 scheelites, by means of linearized augmented plane-wave calculations.¹⁰³
10
11 An analysis of DOS projected on atoms and orbitals shows that the maximum valence band (VB)
12 is derived mostly from O $2p$ orbitals for fundamental and excited states. The CB in the
13 fundamental state is composed of Mo $4d_{xy}$ over $4d_{z^2}$ in the first set of CB and by $4d_{x^2-y^2}$ in the
14 second CB. In the triplet state, it appears new energy levels lower in energy previous this first CB
15 composed by Mo $2 4d_{z^2}$ orbitals which form more $[\text{MoO}_4]$ distorted clusters, as can be seen in
16 the alpha band structure. Some other intermediate levels appear in the uppermost of the VB in the
17 beta band structure, mostly derived from Pb $6p$ orbitals. Figure 8 (b) shows the spin density
18 charge, which is mostly accumulated in Mo $2 4d_{z^2}$ orbitals, so there is a charge transfer from O
19 $2p$ orbitals to empty Mo $2 4d_{z^2}$ orbitals. The rest of CB is found to be governed by Mo $4d_{x^2-y^2}$.
20
21
22
23
24
25
26
27
28
29
30
31
32
33
34
35

36 Insert Figure. 8

37 Therefore, an analysis of site- and orbital-resolved DOS shows a significant dependence of
38 the Mo CB DOS's on local coordination. During the excitation process, some electrons are
39 promoted more feasibly from the oxygen $2p$ states to these molybdenum $4d$ states ($4d_{z^2}$) through
40 the absorption of photons. The emission process of photons occurs when an electron localized in
41 the molybdenum $4d$ state moves into an empty oxygen $2p$ state.
42
43
44
45
46
47

48 The band structure and DOS projected on atoms for singlet and triplet surfaces have also been
49 obtained, and as in the bulk, the formation of intermediary energy levels between CV and CB is
50 favoured by the distortion on $[\text{MoO}_4]_d$ and $[\text{PbO}_8]_d$ clusters. In particular, (001) triplet surface
51 shows a Pb coordinated to six O atoms at distances of 2.40 (x2), 2.42(x2) and 2.65(x2) Å. The
52 spin density is concentrated around the Mo2 atom, which forms the more distorted $[\text{MoO}_4]_d$
53
54
55
56
57
58
59
60

1
2
3 clusters, with the same angles than in the bulk and two distances Mo-O of 1.924 Å and other two
4
5 of 1.835 Å. Such distortion can favour the absence of the (001) facet and then, the growth along
6
7 the [001] direction may lead to the formation of octahedron-like PbMoO₄ microcrystals without
8
9 presence of exposed (001) facets.

10
11 Therefore, the action of acetylacetone and polyvinylpyrrolidone on the PbMoO₄ system would be
12
13 comparable to the localization of an excited state, having as a consequence the formation of
14
15 surface defects and distortions in [MoO₄] or [PbO₈] clusters, which promote remarkable changes
16
17 on the PbMoO₄ morphology.

18 19 **Conclusions**

20
21 In summary, unique PbMoO₄ powders with predominant (111), (100), (011), and (110) facets
22
23 have been prepared using co-precipitation and hydrothermal methods in the presence of
24
25 acetylacetone or polyvinylpyrrolidone with a good control of the synthesis parameters. PbMoO₄
26
27 crystals were characterized by X-ray diffraction (XRD), micro-Raman (MR) spectroscopy, field-
28
29 emission gun scanning electron microscopy (FEG-SEM), and ultraviolet visible absorption
30
31 spectroscopy (UV-vis). The photocatalytic efficiency of powder suspensions of PbMoO₄ micro-
32
33 octahedrons without presence of (001) surface exhibits enhanced activity for the
34
35 photodegradation of rhodamine B (RhB) under ultraviolet-visible light irradiation. The
36
37 surface/bulk defects can influence the separation of photogenerated electron-hole pairs on
38
39 PbMoO₄ under irradiation, and therefore, influence the activity in photocatalytic reaction. There
40
41 is a direct relationship between the surface specific photocatalytic activity and the surface/bulk
42
43 defect. The photocatalytic superiority of this material should be synergistically attributed to its
44
45 high crystallinity, and oriented subunit alignment as well as exposed high-energy (111), (100),
46
47 (011), and (110) facets. The detailed comparison with experimental data shows the high degree of
48
49 agreement and thus we are confident that our findings can provide useful information and can
50
51 serve as a guideline for rational design of PbMoO₄-based materials for various catalytic
52
53 applications.
54
55
56
57
58
59
60

Acknowledgment

The authors thank the financial support from the following Brazilian research financing institutions: CNPq, FAPESP, CAPES, RECAM (Rede de Pesquisa em Catalisadores Ambientais) processo nº 564913/2010-3; MCT/CNPq no 74/2010 and Universal 14/2011 processo nº 481288/2011-2, National Council for Scientific and Technological Development (CNPq), Prometeo/2009/053 (Generalitat Valenciana) and Ministerio de Economía y Competitividad (Spain), CTQ2012-36253-C03-02, and the Spanish–Brazilian program (PHB2009-0065-PC) for their financial support.

Supporting Information: This information is available free of charge via the Internet at <http://pubs.acs.org>

References

- (1) Mikhailik, V. B.; Kraus, H. Performance of Scintillation Materials at Cryogenic Temperatures. *Phys. Status Solidi B*. **2010**, *247*, 1583-1599.
- (2) Mikhailik, V. B.; Kraus, H.; Kapustyanyk, V.; Panasyuk, M.; Prots, Y.; Tsybulskyi, V.; Vasylechko, L. Structure, Luminescence and Scintillation Properties of the MgWO_4 – MgMoO_4 System. *J. Phys.: Condens. Mater.* **2008**, *20*, 365219-36524.
- (3) Ahmad, G.; Dickerson, M. B.; Church, B. C.; Cai, Y.; Jones, S. E.; Naik, R. R.; King, J. S.; Summers, C. J.; Kröger, N.; Sandhage, K. H. Room-Temperature Formation of Crystalline Calcium Molybdate Phosphor Microparticles via Peptide-Induced Precipitation. *Adv. Mater.* **2006**, *18*, 1759-1763.
- (4) Sen, A.; Pramanik, P. A Chemical Synthetic Route for the Preparation of Fine-Grained Metal Molybdate Powders. *Mater. Lett.* **2002**, *52*, 140-146.

- 1
2
3 (5) Guo, C.; Xu, J.; Wang, S.; Li, L.; Zhang, Y.; Li, X. Facile Synthesis and Photocatalytic
4 Application of Hierarchical Mesoporous Bi_2MoO_6 Nanosheet-Based Microspheres.
5 *Cryst. Eng. Comm.* **2012**, *14*, 3602-3608.
6
7
8
9 (6) Duan, F. Z.; Yan, C.; Ming, Q. Enhanced Photocatalytic Activity of Bismuth Molybdate
10 via Hybridization with Carbon. *Mater. Lett.* **2011**, *65*, 191-193.
11
12
13 (7) Li-Qiang, Mai.; F. Y., Yun-Long, Zhao; Xu, Xu; Lin, Xu; Yan-Zhu L. Hierarchical
14 $\text{MnMoO}_4/\text{CoMoO}_4$ Heterostructured Nanowires with Enhanced Supercapacitor
15 Performance. *Nature Commun.* **2011**, *2*, 1-5.
16
17
18 (8) Li, H. C.; Si, W. D.; Wang, R. L.; Xuan, Y.; Liu, B. T.; Xi, X. Dielectric Properties of
19 SrTiO_3 Thin Films Grown on Various Perovskite Electrodes by Pulsed Laser Deposition.
20 *Mat. Sci. Eng. B Solid State Mater. Adv. Technol.* **1998**, *56*, 218-222.
21
22
23 (9) Ding, Y.; Yu, S. H.; Liu, C.; Zang, Z. A. 3D Architectures of Iron Molybdate: Phase
24 Selective Synthesis, Growth Mechanism, and Magnetic Properties. *Chem. Eur. J.* **2007**,
25 *13*, 746-753.
26
27
28 (10) Achary, S. N.; Patwe, S. J.; Mathews, M. D.; Tyagi, A. K. High Temperature Crystal
29 Chemistry and Thermal Expansion of Synthetic Powellite (CaMoO_4): A High
30 Temperature X-ray Diffraction (HT-XRD) Study. *J. Phys. Chem. Solids.* **2006**, *67*, 774-
31 781.
32
33
34 (11) Sun, Y.; Li, C.; Wang, L.; Ma, X.; Zhang, Z.; Song, M.; Ma, P. Synthesis of SrMoO_4
35 Microstructures by the Microwave Radiation-Assisted Chelating Agent Method. *Cryst.*
36 *Res. Technol.* **2011**, *46*, 973-978.
37
38
39 (12) Alves, H.; Hofstaetter, A.; Leiter, F.; Meyer, B. K.; Romanov, N. G.; Novotny, R.;
40 Korzhik, M. V. Green Emitting Molybdate Complexes in PbWO_4 - Results of an ODMR
41 Study. *Radiat. Meas.* **2001**, *33*, 641-644.
42
43
44
45
46
47
48
49
50
51
52
53
54
55
56
57
58
59
60

- 1
2
3 (13) Zhen, L.; Wang, W. S.; Xu, C. Y.; Shao, W. Z.; Ye, M. M.; Chen, Z. L. High
4 Photocatalytic Activity and Photoluminescence Property of Hollow CdMoO₄
5 Microspheres. *Scr. Mater.* **2008**, *58*, 461-464.
6
7
8
9 (14) Groenink, J. A.; Blasse, G. Some New Observation on the Luminescence of PbMoO₄
10 and PbWO₄. *J. Solid State Chem.* **1980**, *32*, 9-20.
11
12
13 (15) Senguttuvan, N.; Babu, S. M.; Subramanian, C. Synthesis, Crystal Growth and
14 Mechanical Properties of Lead Molybdate. *Mater. Sci. Eng. B.* **1997**, *47*, 269-273.
15
16
17 (16) Tyagi, M.; Sangeeta, Desai, D. G.; Sabharwal, S. C. New Observations on the
18 Luminescence of Lead Molybdate Crystals. *J. Lumin.* **2008**, *128*, 22-26.
19
20
21 (17) Errandonea, D. M.; Manjón, F. J.; Santamaria-Perez, D.; Grover, V.; Achary, S. N.;
22 Tyagi, A. K. High-Pressure X-Ray Diffraction Study of Bulk and Nanocrystalline
23 PbMoO₄. *J. Appl. Phys.* **2010**, *108*, 073518-073523.
24
25
26 (18) Spassky, D. A.; Ivanov, S. N.; Kolobanov, V. N.; Mikhailin, V. V.; Zemskov, V. N.;
27 Zadneprovski, B. I.; Potkin, L. I. Optical and Luminescent Properties of the Lead and
28 Barium Molybdates. *Radiat. Meas.* **2004**, *38*, 607-610.
29
30
31 (19) Piwowarska, D.; Kaczmarek, S. M.; Berkowski, M. Dielectric, Optical and EPR Studies
32 of PbMoO₄ Single Crystals, Pure and Doped with Cobalt Ions. *J. Non-Cryst. Solids.*
33 **2008**, *354*, 4437-4442.
34
35
36 (20) Bernhardt, H.; Schnell, R. Modulation-Spectroscopic Investigations of Defect Centres in
37 PbMoO₄ Crystals. *Phys. Status Solidi A* **1981**, *64*, 207-214.
38
39
40 (21) Hofstaetter, A.; Oeder, R.; Scharmann, A.; Schwabe, D.; Vitt, B. Paramagnetic
41 Resonance and Thermoluminescence of the PbWO₄/PbMoO₄ Mixed Crystal System.
42 *Phys. Status Solidi B* **1978**, *89*, 375-380.
43
44
45 (22) Neimann, A. Y.; Afanasiev, A. A.; Feodorova, L. M.; Gabrielian, V. T.; Karagezian, S.
46 M. Deviation from Stoichiometry and Electron Transfer in PbMoO₄. *Phys. Status Solidi*
47 *A.* **1984**, *83*, 153-158.
48
49
50
51
52
53
54
55
56
57
58
59
60

- 1
2
3 (23) Bollmann, W. Coloration, Photoconductivity, Photo and Thermoluminescence of
4
5 PbMoO₄ Crystals. *Krist. und Tech.* **1980**, *15*, 367-375.
6
7 (24) Kudo, A.; Steinberg, M.; Bard, A.; Campion, A.; Fox, M.; Mallouk, T.; Webber, S.;
8
9 White, J. Photoactivity of Ternary Lead-Group IVB Oxides for Hydrogen and Oxygen
10
11 Evolution. *Catal. Lett.* **1990**, *5*, 61-66.
12
13 (25) Zverev, P. G. Vibronic Relaxation of Raman Modes in CaMoO₄ and PbMoO₄ Molecular
14
15 Ionic Crystals *Phys. Status Solidi C.* **2004**, *1*, 3101-3105.
16
17 (26) Kovács, L.; Péter, Á.; Ivleva, L. I.; Baraldi, A.; Capelletti, R. Hydroxyl Ions in Scheelite
18
19 Type Molybdates and Tungstates. *Phys. Status Solidi C.* **2007**, *4*, 856-859.
20
21 (27) Jian-Yu, C.; Qi-Ren, Z.; Ting-Yu, L.; Ze-Xu, S. Electronic Structures of PbMoO₄
22
23 Crystals with F-Type Colour Centres. *Chin. Phys. Lett.* **2007**, *24*, 1660-1663.
24
25 (28) Yevseyev, V. Radiation Effects on Optical Characteristic of PbWO₄. *Int. J. Modern*
26
27 *Phys B* **2008**, *22*, 3695-3707.
28
29 (29) Fujita, M.; Itoh, M.; Mitani, H.; Sangeeta; Tyagi, M. Exciton Transition and Electronic
30
31 Structure of PbMoO₄ Crystals Studied by Polarized Light. *Phys. Status Solidi B.* **2010**, *247*,
32
33 405-410.
34
35 (30) Yang, J. H.; Lu, C. H.; Su, H.; Ma, J. M.; Cheng, H. M.; Qi, L. M. Morphological and
36
37 Structural Modulation of PbWO₄ Crystals Directed by Dextran. *Nanotechnology.* **2008**,
38
39 *19*, 035608- 035615.
40
41 (31) Longo, V. M. *et. al.* A Joint Experimental and Theoretical Study on the
42
43 Nanomorphology of CaWO₄ Crystals. *J. Phys. Chem. C.* **2011**, *115*, 20113-20119.
44
45 (32) Gracia, L.; Longo, V. M.; Cavalcante, L. S.; Beltran, A.; Avansi, W.; Li, M. S.;
46
47 Mastelaro, V. R.; Varela, J. A.; Longo, E.; Andres, J. Presence of Excited Electronic
48
49 State in CaWO₄ Crystals Provoked by a Tetrahedral Distortion: An Experimental and
50
51 Theoretical Investigation. *J. Appl. Phys.* **2011**, *110*, 043501-043512.
52
53
54
55
56
57
58
59
60

- 1
2
3 (33) Bomio, M. R. D.; Cavalcante, L. S.; Almeida, M. A. P.; Tranquilin, R. L.; Batista, N.
4
5 C.; Pizani, P. S.; Siu Li, M.; Andres, J.; Longo, E. Structural Refinement, Growth
6
7 Mechanism, Infrared/Raman Spectroscopies and Photoluminescence Properties of
8
9 PbMoO₄ Crystals. *Polyhedron*. **2013**, *50*, 532-545.
- 10
11 (34) Sczancoski, J. C.; Bomio, M.R.D; Cavalcante, L.S.; Joya, M.R.; Pizani, P.S.; Varela,
12
13 J.A.; Longo, E.; Li Sui M.; Andrés, J.A. Morphology and Blue Photoluminescence
14
15 Emission of PbMoO₄ Processed in Conventional Hydrothermal. *J. Phys. Chem. C*. **2009**,
16
17 *113*, 5812-5822.
- 18
19 (35) Biswas, A.; Bayer, I. S.; Biris, A. S.; Wang, T.; Dervishi, E.; Faupel, F. Advances in
20
21 Top-Down and Bottom-Up Surface Nanofabrication: Techniques, Applications & Future
22
23 Prospects. *Adv. Colloid Interface Sci.* **2012**, *170*, 2-27.
- 24
25 (36) Biao, L.; Shu-Hong, Y.; Linjie, L.; Qiao, Z.; Fen, Z.; Ke, J. Morphology Control of
26
27 Stolzite Microcrystals with High Hierarchy in Solution. *Angew. Chem. Int. Ed.* **2004**, *43*,
28
29 4745-4750.
- 30
31 (37) Shimodaira, Y.; Kato, H.; Kobayashi, H.; Kudo, A. Investigations of Electronic
32
33 Structures and Photocatalytic Activities under Visible Light Irradiation of Lead
34
35 Molybdate Replaced with Chromium[VI]. *Bull. Chem. Soc. Jpn.* 2007, *80*, 885-893.
- 36
37 (38) Cui, X.; Yu, S. H.; Li, L.; Biao, L.; Li, H.; Mo, M.; Liu, X.-M. Selective Synthesis and
38
39 Characterization of Single-Crystal Silver Molybdate/Tungstate Nanowires by a
40
41 Hydrothermal Process. *Chem. Eur. J.* **2004**, *10*, 218-223.
- 42
43 (39) Readman, J. E.; Lister, S. E.; Peters, L.; Wright, J.; Evans, J. S. O. Direct Synthesis of
44
45 Cubic ZrMo₂O₈ Followed by Ultrafast in Situ Powder Diffraction. *J. Am. Chem. Soc.*
46
47 **2009**, *131*, 17560-17562.
- 48
49 (40) Ito, T.; Takagi, H.; Asano, T. Drastic and Sharp Change in Color, Shape, and
50
51 Magnetism in Transition of CuMoO₄ Single Crystals. *Chem. Mater.* **2009**, *21*, 3376-
52
53 3379.
- 54
55
56
57
58
59
60

- 1
2
3 (41) Zeng, H. C. Synthesis of Stoichiometric Lead Molybdate PbMoO_4 : An X-Ray
4
5 Diffraction, Fourier Transform Infrared Spectroscopy, and Differential Thermal Analysis
6
7 Study. *J. Mater. Res.* **1996**, *11*, 703-715.
8
- 9 (42) Arkady, Y.; Neiman, A. F. G.; Sharafutdinov, A. R. Origin of Potential Difference Self
10
11 Generated by Reaction and Transport Processes. *Solid State Ionics.* **1997**, *367*, 101-103.
12
- 13 (43) Zeng, H. C. Rectangular Vacancy Island Formation and Self-Depletion in Czochralski-
14
15 grown PbMoO_4 Single Crystal During Heat Treatment. *J. Cryst. Growth.* **1996**, *160*, 119-
16
17 128.
18
- 19 (44) Nakamura, T.; Sugiyama, K.; Moriguchi, E.; Shoji, T. Synthesis of Scheelite Group
20
21 Minerals in the CaWO_4 - CaMoO_4 - PbMoO_4 - PbWO_4 System from Aqueous Solutions
22
23 at 100°C . *J. Min. Mater. Process. Inst. Jpn.* **2002**, *118*, 217-221.
24
25
- 26 (45) Pandey, P. K.; Bhave, N. S.; Kharat, R. B. Structural, Optical, Electrical and
27
28 Photovoltaic Electrochemical Studies of Cobalt Molybdates Thin Films. *Indian J. Pure*
29
30 *& Appl. Phys.* **2006**, *44*, 52-58.
31
- 32 (46) Ryu, J. H.; Koo, S. M.; Yoon, J. W.; Lim, C. S.; Shim, K. B. Synthesis of
33
34 Nanocrystalline MMoO_4 ($M = \text{Ni}, \text{Zn}$) Phosphors Via a Citrate Complex Route Assisted
35
36 by Microwave Irradiation and Their Photoluminescence. *Mater. Lett.* **2006**, *60*, 1702-
37
38 1705.
39
- 40 (47) Phuruangrat, A.; Thongtem, T.; Thongtem, S. Analysis of Lead Molybdate and Lead
41
42 Tungstate Synthesized by a Sonochemical Method. *Curr. Appl. Phys.* **2010**, *10*, 342-345.
43
- 44 (48) Kianpour, G.; Salavati-Niasari, M.; Emadi, H. Sonochemical Synthesis and
45
46 Characterization of NiMoO_4 Nanorods. *Ultrason. Sonochem.* **2013**, *20*, 418-424.
47
48
- 49 (49) Di Chen, G. S.; Kaibin, T.; Zhenhua, L.; Huagui, Z. AOT-Microemulsions-Based
50
51 Formation and Evolution of PbWO_4 Crystals. *J. Phys. Chem. B.* **2004**, *108*, 11280-
52
53 11284.
54
55
56
57
58
59
60

- 1
2
3 (50) Phuruangrat, A.T.; Thongtem, T.; Somchai, T. Synthesis of Lead Molybdate and Lead
4 Tungstate via Microwave Irradiation Method. *J. Cryst. Growth*. **2009**, *311*, 4076-4081.
5
6
7 (51) Thongtem, T.; Kungwankunakorn, S.; Kuntalue, B.; Phuruangrat, A.; Thongtem, S.
8 Luminescence and Absorbance of Highly Crystalline CaMoO_4 , SrMoO_4 , CaWO_4 and
9 SrWO_4 Nanoparticles Synthesized by Co-Precipitation Method at Room Temperature. *J.*
10 *Alloys Compd.* **2010**, *506*, 475-481.
11
12
13 (52) Kianpour, G.; Salavati-Niasari, M.; Emadi, H. Precipitation Synthesis and
14 Characterization of Cobalt Molybdates Nanostructures. *Superlattices Microstruct.* **2013**,
15 *58*, 120-129.
16
17
18 (53) Cheng, Y.; Wang, Y.; Chen, D.; Bao, F. Evolution of Single Crystalline Dendrites from
19 Nanoparticles Through Oriented Attachment. *J. Phys. Chem. B*. **2005**, *109*, 794-798.
20
21
22 (54) Shen, M.; Zhang, Q.; Chen, H.; Peng, T. Hydrothermal Fabrication of PbMoO_4
23 Microcrystals with Exposed (001) Facets and its Enhanced Photocatalytic Properties.
24 *Cryst. Eng. Comm.* **2011**, *13*, 2785-2791.
25
26
27 (55) Hashim, M.; Hu, C.; Wang, X.; Li, X.; Guo, D. Synthesis and Photocatalytic Property
28 of Lead Molybdate Dendrites with Exposed (001) facet. *Appl. Surf. Sci.* **2012**, *258*, 5858-
29 5862.
30
31
32 (56) Xing, G. J.; Liu, R.; Zhao, C.; Li, Y. L.; Wang, Y.; Wu, G. M. Photoluminescence and
33 Photocatalytic Properties of Uniform PbMoO_4 Polyhedral Crystals Synthesized by
34 Microemulsion-Based Solvothermal Method. *Ceram. Int.* **2011**, *37*, 2951-2956.
35
36
37 (57) Hernández-Uresti, D. B.; Martínez-de la Cruz, A.; Torres-Martínez, L. Photocatalytic
38 Properties of PbMoO_4 Synthesized by Co-Precipitation Method: Organic Dyes
39 Degradation under UV Irradiation. *Res. Chem. Intermed.* **2012**, *38*, 817-828.
40
41
42 (58) Martínez-de la Cruz, A.; Hernández-Uresti, D. B.; Torres-Martínez, L.; Lee, S. W.
43 Photocatalytic Properties of PbMoO_4 Synthesized by a Hydrothermal Reaction. *Reac.*
44 *Kinet. Mech. Cat.* **2012**, *107*, 467-475.
45
46
47
48
49
50
51
52
53
54
55
56
57
58
59
60

- 1
2
3 (59) Dickinson, R. G. The Crystal Structure of Wulfenite and Scheelite. *J. Am. Chem. Soc.*
4
5 **1920**, *42*, 85-93.
6
7 (60) Gibbs, J. W.; Smith, A. W. On the Equilibrium of Heterogeneous Substances.
8
9 *Transactions of the Connecticut Academy of Arts and Sciences* **1874**, *3*, 343-324.
10
11 (61) Wulff, G. Zur Frage der Geschwindigkeit Des Wachstums und Der Auflosung der
12
13 Krystallflächen. *Z. Kristallogr. Mineral* **1901**, *34*, 1-8.
14
15 (62) Von Laue, M. Der Wulffsche Satz für Die Gleichgewichtsform von Kristallen.
16
17 *Kristallogr. die Gleichgewichtsform von Kristallen. Z. Kristallogr.* **1943**, *105*, 124-133.
18
19 (63) Herring, C. Some Theorems on the Free Energies of Crystal Surfaces. *Phys. Rev.* **1951**,
20
21 *82*, 87-93.
22
23 (64) Sun, C. Q. Size Dependence of Nanostructures: Impact of Bond Order Deficiency. *Solid*
24
25 *State Chem.* **2007**, *35*, 1-159.
26
27 (65) Sun, C. Q. Dominance of Broken Bonds and Nonbonding Electrons at the Nanoscale.
28
29 *Nanoscale.* **2010**, *2*, 1930-1961.
30
31 (66) Liu, X. J.; Li, J. W.; Zhou, Z. F.; Yang, L. W.; Ma, Z. S.; Xie, G. F.; Pan, Y.; Sun, C. Q.
32
33 Size-Induced Elastic Stiffening of ZnO Nanostructures: Skin-Depth Energy Pinning.
34
35 *Appl. Phys. Lett.* **2009**, *94*, 131902-131905.
36
37 (67) Marks, L. D. Modified Wulff Constructions for Twinned Particles. *J. Cryst. Growth*
38
39 **1983**, *61*, 556-566.
40
41 (68) Gracia, L.; Beltrán, A.; Andrés, J. Characterization of the High-Pressure Structures and
42
43 Phase Transformations in SnO₂. A Density Functional Theory Study. *J. Phys. Chem. B*
44
45 **2007**, *111*, 6479-6485.
46
47 (69) Stroppa, D. G. *et. al.* Unveiling the Chemical and Morphological Features of Sb-SnO₂
48
49 Nanocrystals by the Combined Use of High-Resolution Transmission Electron
50
51 Microscopy and ab Initio Surface Energy Calculations. *J. Am. Chem. Soc.* **2009**, *131*,
52
53 14544-14548.
54
55
56
57
58
59
60

- 1
2
3 (70) Gracia, L.; Andrés, J.; Longo, V. M.; Varela, J. A.; Longo, E. A Theoretical Study on
4 the Photoluminescence of SrTiO₃. *Chem. Phys. Lett.* **2010**, *493*, 141-146.
5
6
7 (71) Itoh, M.; Kajitani, T. Polarized Luminescence from Jahn-Teller Split Triplet States of
8 Self-Trapped Excitons in PbMoO₄. *Phys. Rev. B.* **2013**, *87*, 085201-085208.
9
10
11 (72) Wong-Ng, W.; McMurdie, H. F., Hubbard, C. R.; Mighell, A. D. JCPDS-ICDD
12 Research Associateship (Cooperative Program with NBS/NIST). *J. Res. Natl. Inst.*
13 *Stand. Technol.* **2001**, *106*, 1013–1028.
14
15
16
17 (73) Lutterotti, L. Total Pattern Fitting for the Combined Size–Strain–Stress–Texture
18 Determination in Thin Film Diffraction. *Nucl. Instrum. Methods B.* **2010**, *268*, 334-340.
19
20
21 (74) Lutterotti, L.; Bortolotti, M.; Ischia, G.; Lonardelli, I.; Wenk, H. R. Rietveld Texture
22 Analysis from Diffraction Images. *Z. Kristallogr. Suppl.* **2007**, *2007*, 125-130.
23
24
25
26 (75) Rousseau, D. L.; Baumann, R. P.; Porto, S. P. S. Normal Mode Determination in
27 Crystals. *J. Raman Spectros.* **1981**, *10*, 253-290.
28
29
30
31 (76) Porto, S. P. S.; Scott, J. F. Raman Spectra of CaWO₄, SrWO₄, CaMoO₄, and SrMoO₄.
32 *Phys. Rev.* **1967**, *157*, 716-719.
33
34
35 (77) Ling, Z. C.; Xia, H. R.; Ran, D. G.; Liu, F. Q.; Sun, S. Q.; Fan, J. D.; Zhang, H. J.;
36 Wang, J. Y.; Yu, L. L. Lattice Vibration Spectra and Thermal Properties of SrWO₄
37 Single Crystal. *Chem. Phys. Lett.* **2006**, *426*, 85-90.
38
39
40
41 (78) Basiev, T. T.; Sobol, A. A.; Voronko, Y. K.; Zverev, P. G. Spontaneous Raman
42 Spectroscopy of Tungstate and Molybdate Crystals for Raman Lasers. *Opt. Mater.* **2000**,
43 *15*, 205-216.
44
45
46
47 (79) Yu, C. L.; *et. al.* Structural and Electrical Properties of PbMoO₄ Under High Pressure. *J.*
48 *Phys. Condens. Matt.* **2007**, *19*, 425215-425222.
49
50
51
52 (80) Jayaraman, A.; Batlogg, B.; Van Uitert L. G. Effect of High Pressure on the Raman and
53 Electronic Absorption Spectra of PbMoO₄ and PbWO₄. *Phys. Rev. B.* **1985**, *31*, 5423-
54 5427.
55
56
57
58
59
60

- 1
2
3 (81) Moraes, E.; Bomio, M. R. D.; Longo, V. M.; Longo, E.; Varela, J. A. Freezing
4 Distortions and Photoluminescence Property in PbMoO₄ Micro-Octahedrons: An
5 Experimental and Theoretical Study. *Curr. Phys. Chem.* **2013**, *3*, In Press.
6
7
8
9 (82) Basiev, T. T.; Vassiliev, S. V.; Konjushkin, V. A.; Osiko, V. V.; Zagumennyi, A. I.;
10 Zavartsev, Y. D.; Kutovoi, S. A.; Shcherbakov, I. A. Diode Pumped 500-Picosecond
11 Nd:GdVO₄ Raman Laser. *Laser Phys. Lett.* **2004**, *1*, 237-240.
12
13
14 (83) Voron'ko, Y. K.; Sobol', A. A.; Shukshin, V. E.; Zagumennyi, A. I.; Zavartsev, Y. D.;
15 Kutovoi, S. A. Raman Spectroscopic Study of Structural Disordering in YVO₄, GdVO₄,
16 and CaWO₄ Crystals. *Phys. Solid State* **2009**, *51*, 1886-1893.
17
18
19 (84) See <http://www.jcrystal.com/steffenweber/JAVA/JSV/jsv.html>.
20
21
22 (85) See <http://www.km.kongsberg.com/sim>.
23
24
25 (86) Yang, W. D.; Haile, S. M. Influences of Water Content on Synthesis of (Pb_{0.5}Ba_{0.5})TiO₃
26 Materials Using Acetylacetone as Chelating Agent in a Sol–Gel Process. *J. Eur. Cera.*
27 *Soc.* **2006**, *26*, 3203-3210.
28
29
30 (87) Raykar, V. S.; Singh, A. K. Thermal and Rheological Behavior of Acetylacetone
31 Stabilized ZnO Nanofluids. *Therm. Acta.* **2010**, *502*, 60-65.
32
33
34 (88) Uchiyama, H.; Takagi, K.; Kozuka, H. Solvothermal Synthesis of Size-Controlled ZrO₂
35 Microspheres via Hydrolysis of Alkoxides Modified with Acetylacetone. *Colloids Surf.*
36 *A: Physicochem. Eng. Aspects.* **2012**, *403*, 121-128.
37
38
39 (89) Weng, L.; Bao, X.; Sagoe-Crentsil, K. Effect of Acetylacetone on the Preparation of
40 PZT Materials in Sol–Gel Processing. *Mater. Sci. Eng.: B.* **2002**, *96*, 307-312.
41
42
43 (90) Penn, R. L.; Banfield, J. F. Morphology Development and Crystal Growth in
44 Nanocrystalline Aggregates under Hydrothermal Conditions: Insights from Titania.
45 *Geochim. Cosmochim. Acta.* **1999**, *63*, 1549-1557.
46
47
48 (91) Penn, R. L.; Banfield, J. F. Imperfect Oriented Attachment: Dislocation Generation in
49 Defect-Free Nanocrystals. *Science* **1998**, *281*, 969-971.
50
51
52
53
54
55
56
57
58
59
60

- 1
2
3 (92) Wu, X.; Du, J.; Li, H.; Zhang, M.; Xi, B.; Fan, H.; Zhu, Y.; Qian, Y. Aqueous
4 Mineralization Process to Synthesize Uniform Shuttle-Like BaMoO₄ Microcrystals at
5 Room Temperature. *J. Solid State Chem.* **2007**, *180*, 3288-3295.
6
7
8
9 (93) Ryu, E. K.; Huh, Y. D. Synthesis of Hierarchical Self-Assembled BaMoO₄
10 Microcrystals. *Bull. Korean Chem. Soc.* **2008**, *29*, 503-506.
11
12
13 (94) Scopece, D. SOWOS: An Open-Source Program for the Three-Dimensional Wulff
14 Construction. *J. Appl. Crystallogr.* **2013**, *46*, 811-816.
15
16
17 (95) Chu, H.; Li, X.; Chen, G.; Jin, Z.; Zhang, Y.; Li, Y. Inorganic Hierarchical
18 Nanostructures Induced by Concentration Difference and Gradient. *Nano Res.* **2008**, *1*,
19 213-220.
20
21
22 (96) Wood, D. L.; Tauc, J. Weak Absorption Tails in Amorphous Semiconductors. *Phys.*
23 *Rev. B* 1972, *5*, 3144-3151.
24
25
26 (97) Lacomba-Perales, R.; Ruiz-Fuertes, J.; Errandonea, D.; Martínez-García, D.; Segura, A.
27 Optical Absorption of Divalent Metal Tungstate: Correlation Between the Band-Gap
28 Energy and the Cation Ionic Radius. *Europhys. Lett.* **2008**, *83*, 37002-37007.
29
30
31 (98) Longo, V. M.; Cavalcante, L. S.; Paris, E. C.; Sczancoski, J. C.; Pizani, P. S.; Li, M. S.;
32 Andrés, J.; Longo, E.; Varela, J. A. Hierarchical Assembly of CaMoO₄ Nano-
33 Octahedrons and Their Photoluminescence Properties. *J. Phys.Chem.C.* **2011**, *115*, 5207-
34 5919.
35
36
37 (99) Hernández-Uresti, D.; Martínez-de la Cruz, A.; Torres-Martínez, L. Photocatalytic
38 Properties of PbMoO₄ Synthesized by Co-Precipitation method: Organic Dyes
39 Degradation under UV Irradiation. *Res. Chem. Intermed.* **2012**, *38*, 817-828.
40
41
42 (100) Chen, Q.; Wu, Q. Fabrication of Carbon Microspheres@PbMoO₄ Core-Shell Hybrid
43 Structures and Its Visible Light-Induced Photocatalytic Activity. *Catal. Commun.* **2012**,
44 *24*, 85-89.
45
46
47
48
49
50
51
52
53
54
55
56
57
58
59
60

- 1
2
3 (101) Dai, K.; Yao, Y.; Liu, H.; Mohamed, I.; Chen, H.; Huang, Q. Enhancing the
4
5 Photocatalytic Activity of Lead Molybdate by Modifying with Fullerene. *J. Mol. Catal.*
6
7 *A: Chem.* **2013**, *375*, 111-117.
8
- 9 (102) Cavalcante, L. S.; Sczancoski, J. C.; Batista, N. C.; Longo, E.; Varela, J. A.; Orlandi,
10
11 M. O. Growth Mechanism and Photocatalytic Properties of SrWO₄ Microcrystals
12
13 Synthesized by Injection of Ions into a Hot Aqueous Solution. *Adv. Powder Technol.*
14
15 **2013**, *24*, 344-353.
16
- 17 (103) Zhang, Y.; Holzwarth, N. A. W.; Williams, R. T. Electronic Band Structures of the
18
19 Scheelite Materials CaMoO₄, CaWO₄, PbMoO₄, and PbWO₄. *Phys. Rev. B* **1998**, *57*,
20
21 12738-12750.
22
23
24
25
26
27
28
29
30
31
32
33
34
35
36
37
38
39
40
41
42
43
44
45
46
47
48
49
50
51
52
53
54
55
56
57
58
59
60

Table Caption

Table 1. Rietveld refined parameters of PMO/acac and PMO/PVP processed in a hydrothermal system at 100 °C for 10 min.

PMO	a (Å)	c (Å)	c/a	Cell volume (Å ³)	χ^2	R-Bragg (%)	Rwp (%)
JCPDS 44-1486	5.433	12.110	2.228	357.456	-	-	-
acac 100°C/10min	5.439	12.124	2.229	358.661	2.70	8.76	4.32
PVP 100°C/10min	5.438	12.124	2.229	358.529	2.28	7.53	4.55

χ^2 , goodness of fit; Rwp, weighted error (%).

Table 2. Number of PbMoO₄ units, area, surface energy and band gap energy for (001), (100), (110), (101) and (111) surfaces of PbMoO₄. All surfaces are O-terminated.

	n	Area (Å ²)	E _{surf} (J·m ⁻²)	relax(%)	E _{gap} (eV)
bulk	2				3.70
[001]	5	30.07	0.28	33.2	3.58
[100]	8	66.84	0.37	63.8	3.99
[110]	5	47.26	0.58	75.5	3.61
[101]	4	36.65	0.66	64.8	3.86
[111]	10	99.20	0.61	60.4	3.60

Table 3. Comparative results between the E_{gap} values of PbMoO_4 obtained in this work and those reported in literature by different synthesis methods.

Method	Temperature (°C)	time (min)	E_{gap} (eV)	Ref.
Reflux Method		1440	3.31	37
Hydrothermal	180	1440	3.21	24
Co-precipitation/ thermal treatment	350	1440	3.16	99
Solid-state reaction	950	4320	3.1	20
Solvothermal	160	720	3.3	12
Hydrothermal/acac	100	10	3.05	This work
Hydrothermal/PVP	100	10	3.17	This work

Figure Caption

Figure 1. XRD patterns of PbMoO₄/acac and PbMoO₄/PVP micro-octahedrons processed by hydrothermal method at 100°C for 10min.

Figure 2. Micro Raman spectra in the range from 50 to 1000 cm⁻¹ of PbMoO₄/acac and PbMoO₄/PVP micro-octahedrons processed by hydrothermal method at 100°C for 10min.

(T) = Theoretical Raman modes of the triplet state.

Figure 3. FEG-SEM micrographs of PbMoO₄ micro-octahedrons processed by hydrothermal method at 100°C/10 min (a, b) PMO/acac and (c,d) PMO/PVP.

Figure 4. Schematic representation of the synthesis and growth mechanism for PbMoO₄ crystals by FEG-SEM (1) without modifiers, (2) with acetylacetone (acac) and (3) polyvinylpyrrolidone (PVP).

Figure 5. Geometry of optimized surfaces a) (001), b) (100), c) (110), d) (101) and e) (111).

Figure 6. Wulff constructed nanocrystal using SOWOS code.⁹⁴

Figure 7. UV-vis absorption spectra for (a) PMO/WS, (b) PMO/acac and (c) PMO/PVP micro-octahedrons during different exposure time of illumination for the photodegradation of RhB dye. Inset shows photodegradation efficiencies of RhB as a function of irradiation time for different photocatalysts.

Figure 8. Calculated band structure and total DOS projected on atoms of triplet PMO (a) and the spin charge density location in the unit cell of triplet PMO (b).

Figure 1

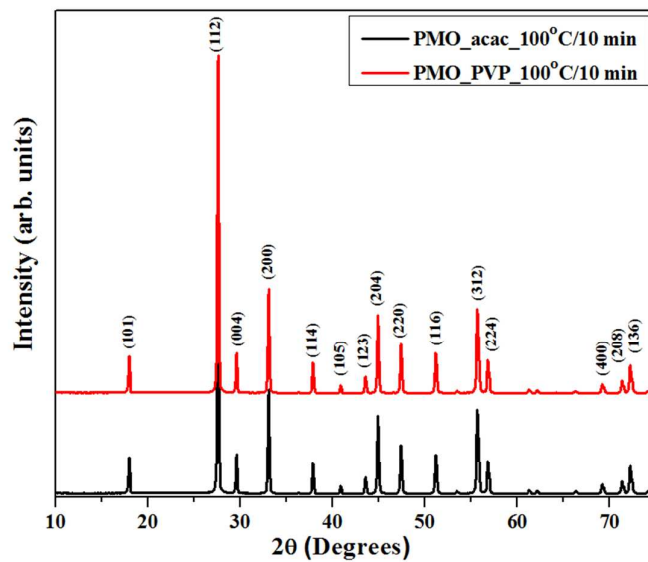


Figure 2

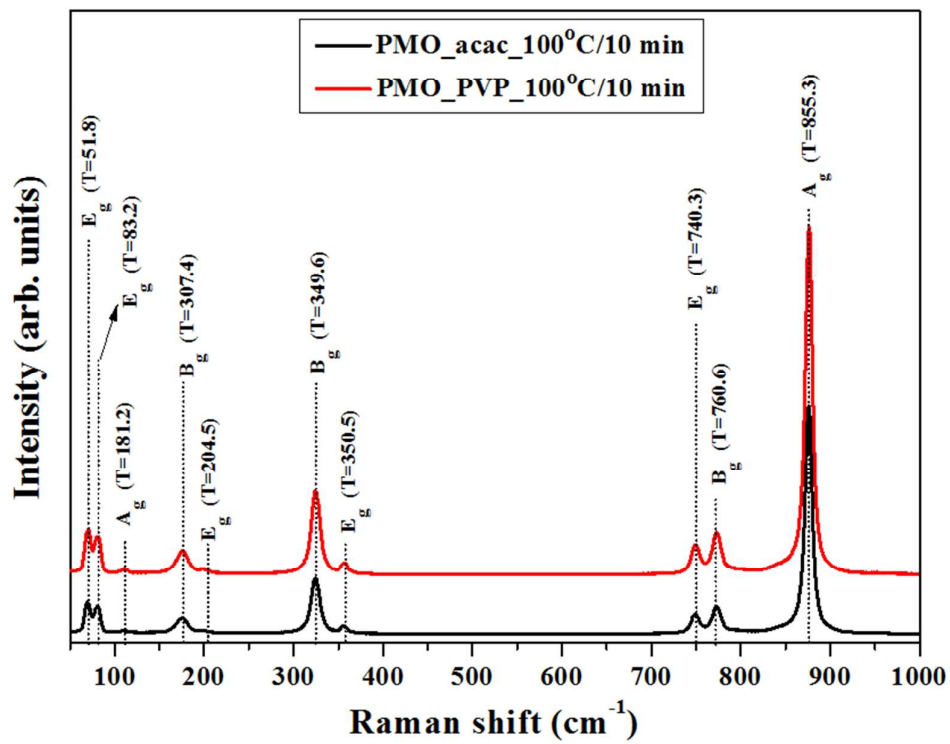


Figure 3

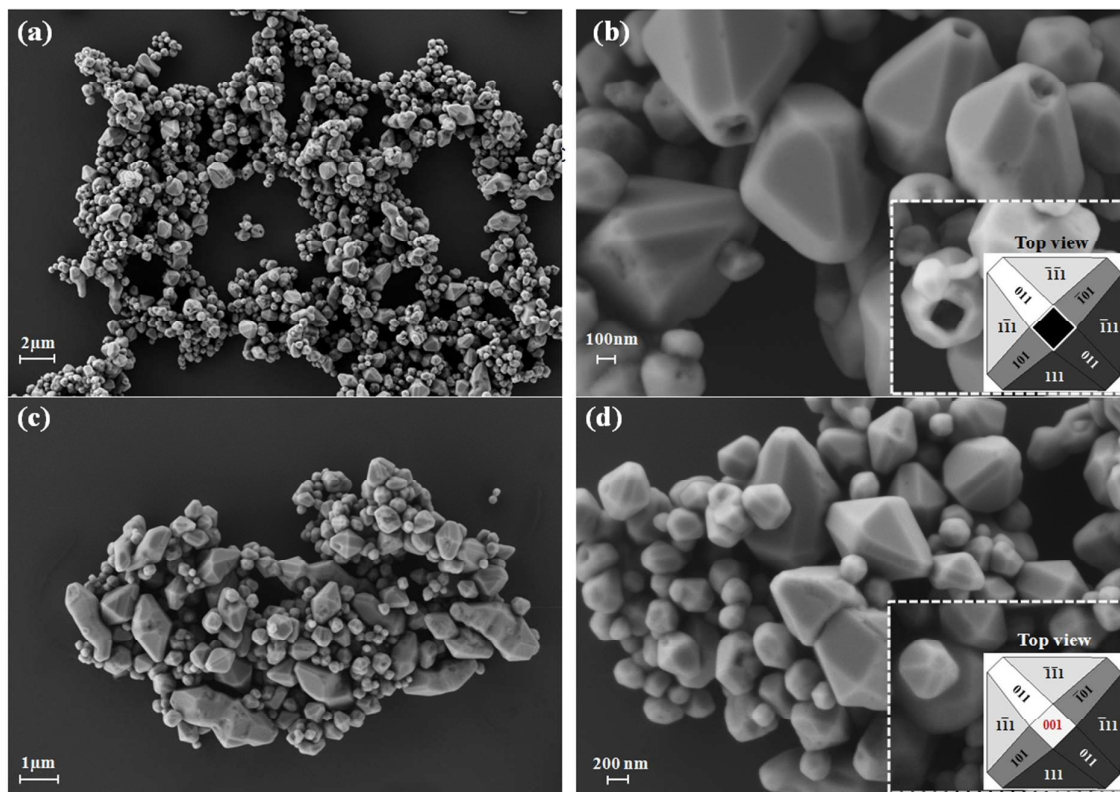


Figure 4

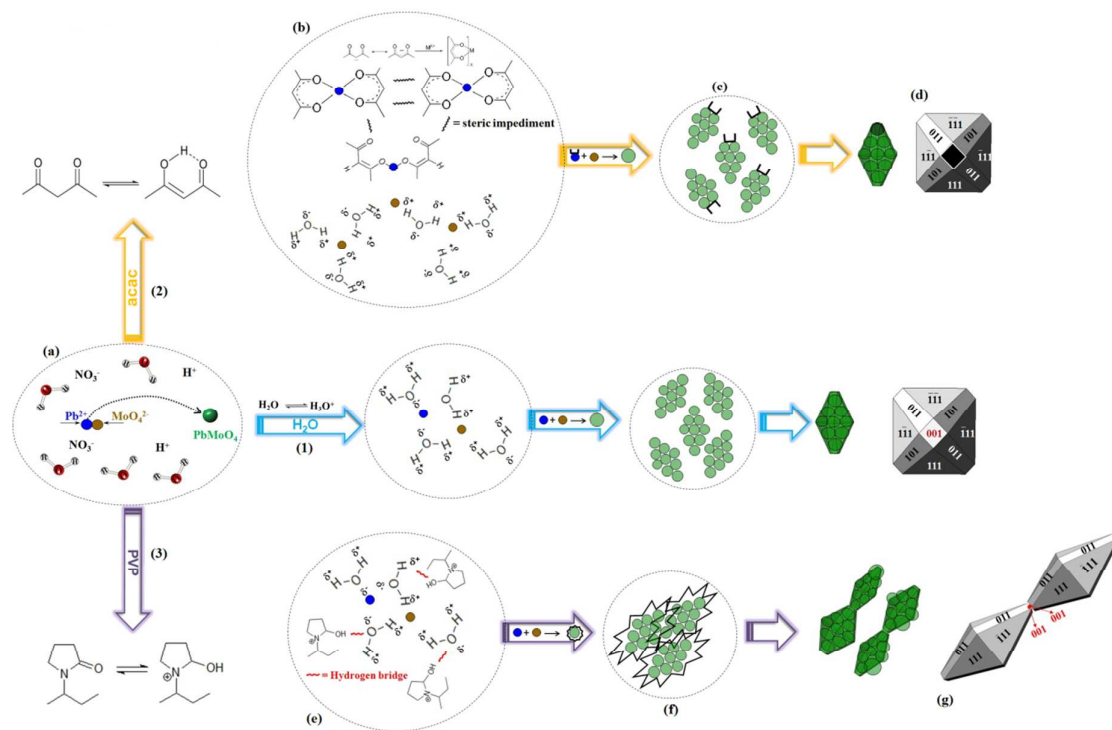


Figure 5.

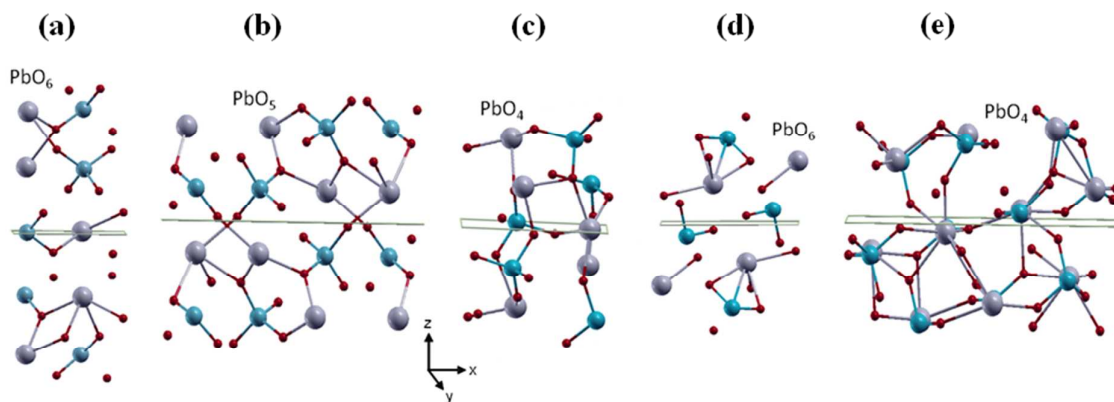


Figure 6.

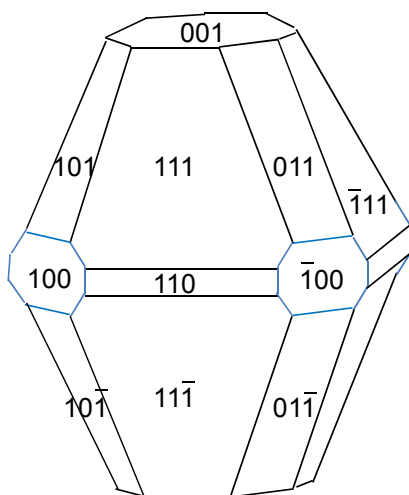


Figure 7

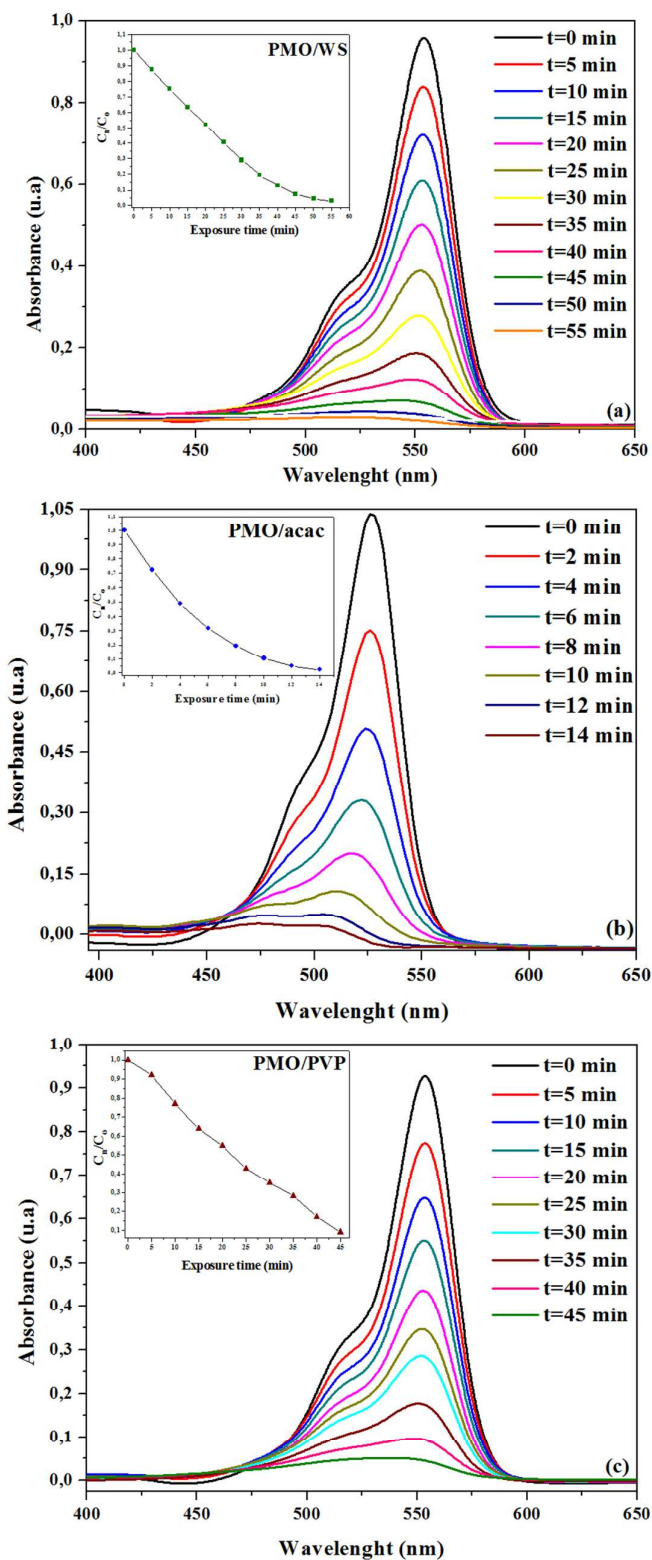
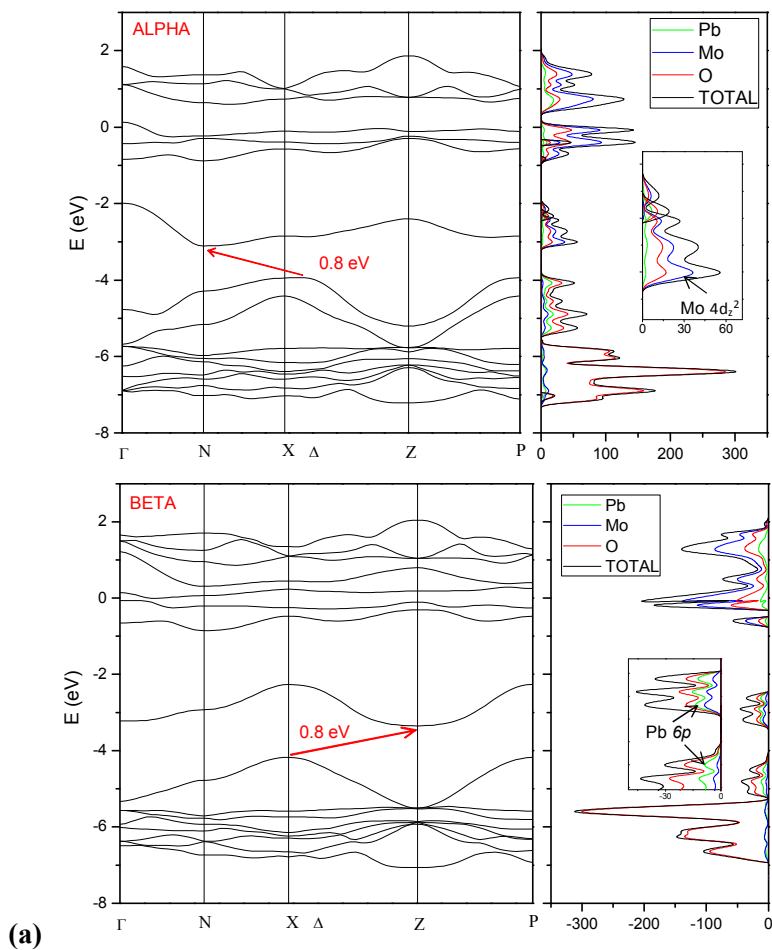
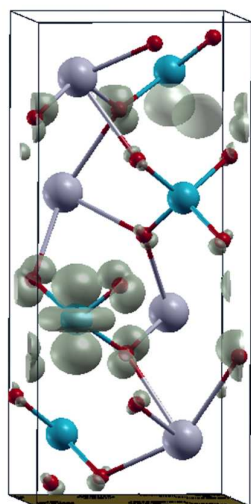


Figure 8

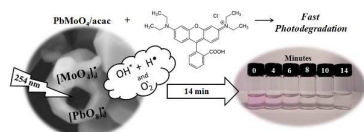


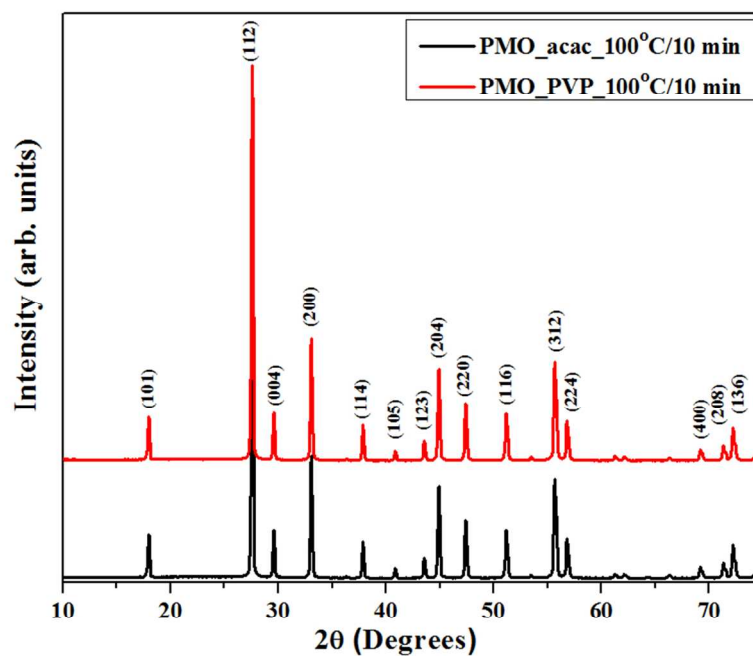
(a)



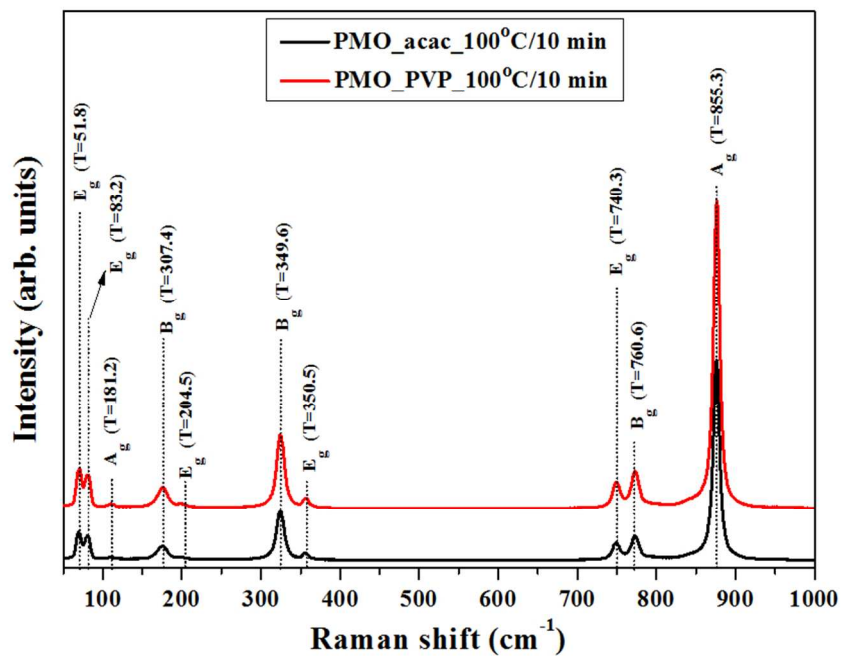
(b)

Table of Contents



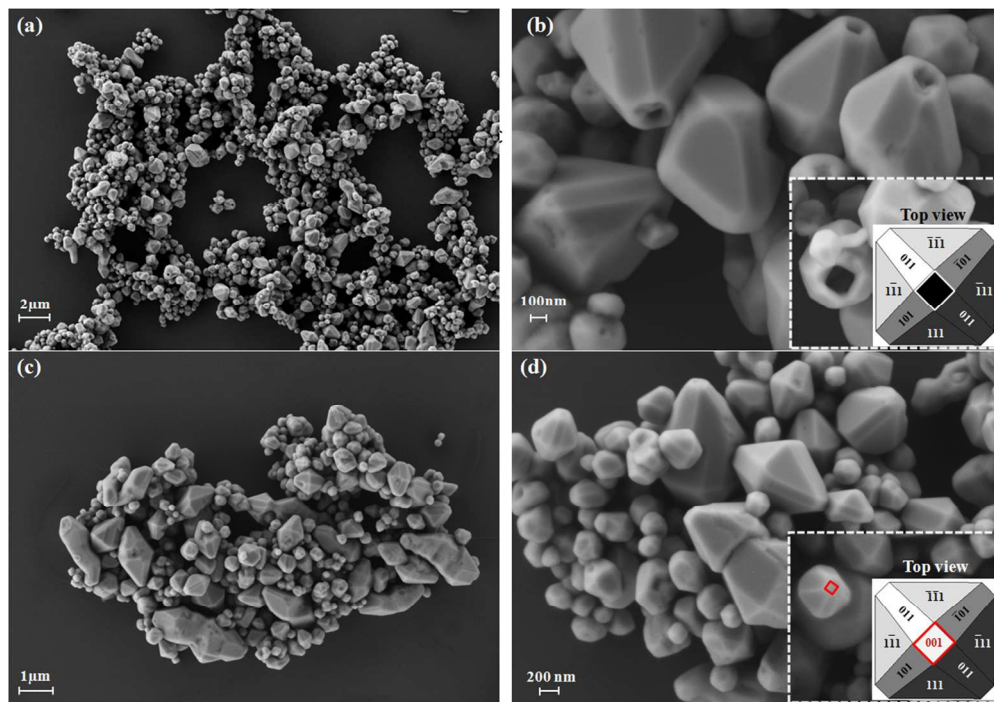


XRD patterns of PbMoO₄/acac and PbMoO₄/PVP micro-octahedrons processed by hydrothermal method at 100°C for 10 min.
263x220mm (96 x 96 DPI)

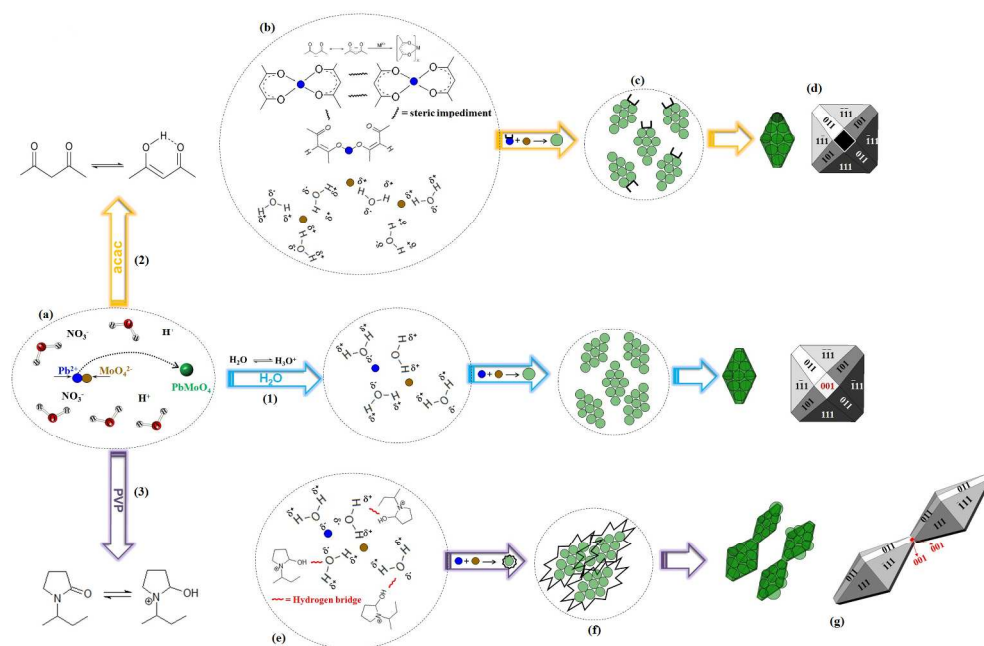


Micro Raman spectra in the range from 50 to 1000 cm⁻¹ of PbMoO₄/acac and PbMoO₄/PVP micro-octahedrons processed by hydrothermal method at 100°C for 10 min. (T) = Theoretical Raman modes of the triplet state.

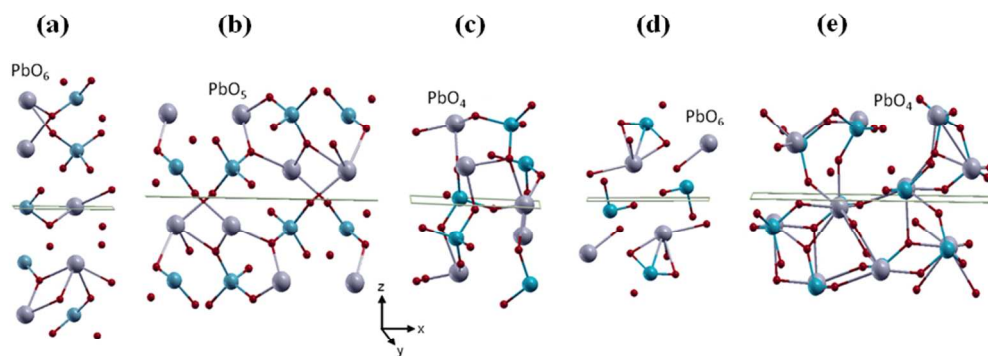
263x220mm (96 x 96 DPI)



FEG-SEM micrographs of PbMoO_4 micro-octahedrons processed by hydrothermal method at $100^\circ\text{C}/10$ min
(a, b) PMO/acac and (c,d) PMO/PVP.
322x226mm (96 x 96 DPI)

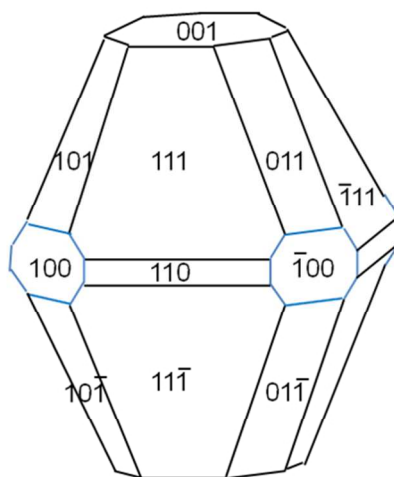


Schematic representation of the synthesis and growth mechanism for PbMoO_4 crystals by FEG-SEM (1) without modifiers, (2) with acetylacetone (acac) and (3) polyvinylpyrrolidone (PVP).
674x431mm (96 x 96 DPI)

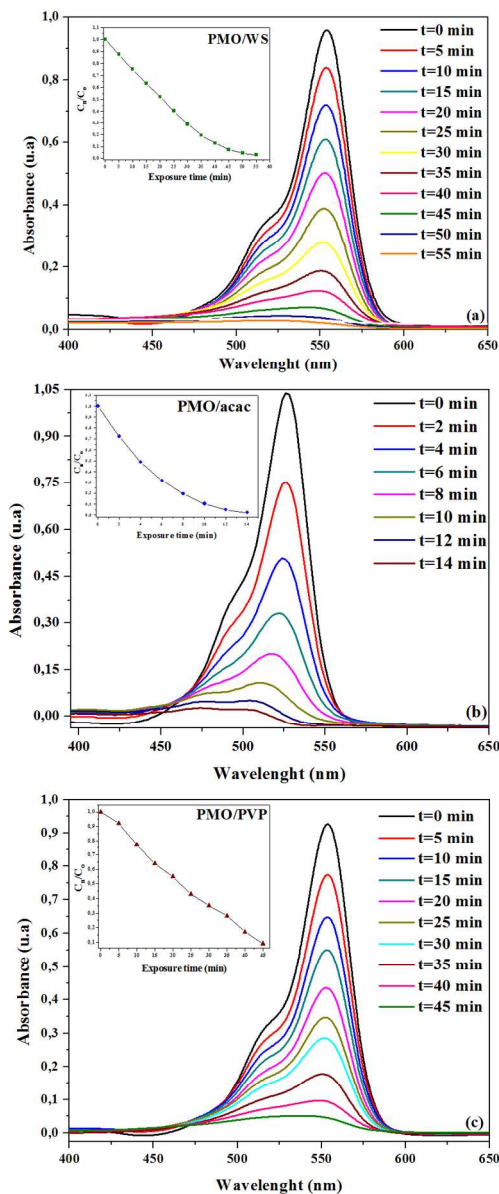


32
33
34
35
36
37
38
39
40
41
42
43
44
45
46
47
48
49
50
51
52
53
54
55
56
57
58
59
60

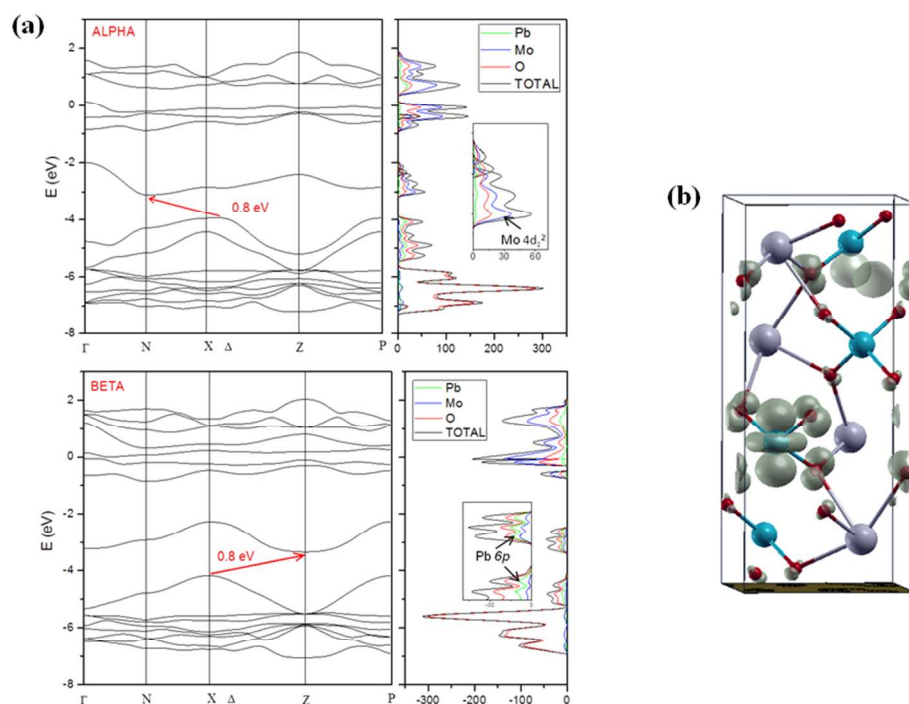
Geometry of optimized surfaces a) (001), b) (100), c) (110), d) (101) and e) (111).
254x190mm (96 x 96 DPI)



Wulff constructed nanocrystal using SOWOS code.
254x190mm (96 x 96 DPI)



UV-vis absorption spectra for (a) PMO/WS, (b) PMO/acac and (c) PMO/PVP micro-octahedrons during different exposure time of illumination for the photodegradation of RhB dye. Inset shows photodegradation efficiencies of RhB as a function of irradiation time for different photocatalysts.
406x563mm (96 x 96 DPI)



Calculated band structure and total DOS projected on atoms of triplet PMO (a) and the spin charge density location in the unit cell of triplet PMO (b).
254x190mm (96 x 96 DPI)

1
2
3 **Table Caption**
4
5

6 **Table 1.** Rietveld refined parameters of PMO/acac and PMO/PVP processed in a hydrothermal
7 system at 100 °C for 10 min.
8
9

10
11
12
13
14

PMO	a (Å)	c (Å)	c/a	Cell volume (Å ³)	χ^2	R-Bragg (%)	Rwp (%)
JCPDS 44-1486	5.433	12.110	2.228	357.456	-	-	-
acac 100°C/10min	5.439	12.124	2.229	358.661	2.70	8.76	4.32
PVP 100°C/10min	5.438	12.124	2.229	358.529	2.28	7.53	4.55

15
16
17
18
19
20
21
22
23
24
25
26
27
28
29
30
31
32
33
34
35
36
37
38 χ^2 , goodness of fit; Rwp, weighted error (%).
39
40
41
42
43
44
45
46
47
48
49
50
51
52
53
54
55
56
57
58
59
60

Table 2. Number of PbMoO₄ units, area, surface energy and band gap energy for (001), (100), (110), (101) and (111) surfaces of PbMoO₄. All surfaces are O-terminated.

	n	Area (Å ²)	E _{surf} (J·m ⁻²)	relax(%)	E _{gap} (eV)
bulk	2				3.70
[001]	5	30.07	0.28	33.2	3.58
[100]	8	66.84	0.37	63.8	3.99
[110]	5	47.26	0.58	75.5	3.61
[101]	4	36.65	0.66	64.8	3.86
[111]	10	99.20	0.61	60.4	3.60

Table 3. Comparative results between the E_{gap} values of PbMoO_4 obtained in this work and those reported in literature by different synthesis methods.

Method	Temperature (°C)	time (min)	E_{gap} (eV)	Ref.
Reflux Method		1440	3.31	104
Hydrothermal	180	1440	3.21	24
Co-precipitation/ thermal treatment	350	1440	3.16	99
Solid-state reaction	950	4320	3.1	20
Solvothermal	160	720	3.3	12
Hydrothermal/acac	100	10	3.05	This work
Hydrothermal/PVP	100	10	3.17	This work